A Closer Look at Personalized Fine-Tuning in Heterogeneous Federated Learning

Anonymous authors
Paper under double-blind review

Abstract

Federated Learning (FL) enables decentralized, privacy-preserving model training but struggles to balance global generalization and local personalization due to non-identical data distributions across clients. Personalized Fine-Tuning (PFT), a popular post-hoc solution, fine-tunes the final global model locally but often overfits to skewed client distributions or fails under domain shifts. We propose adapting Linear Probing followed by full Fine-Tuning (LP-FT)—a principled centralized strategy for alleviating feature distortion (Kumar et al., 2022)—to the FL setting. Through systematic evaluation across seven datasets and six PFT variants, we demonstrate LP-FT's superiority in balancing personalization and generalization. Our analysis uncovers federated feature distortion, a phenomenon where local fine-tuning destabilizes globally learned features, and theoretically characterizes how LP-FT mitigates this via phased parameter updates. We further establish conditions (e.g., partial feature overlap, covariate-concept shift) under which LP-FT outperforms standard fine-tuning, offering actionable guidelines for deploying robust personalization in FL.

1 Introduction

Federated Learning (FL) (McMahan et al., 2017) enables collaborative learning from decentralized data while preserving privacy, typically by training a shared global model, referred to as General FL (GFL). However, variations in client data distributions often limit GFL's effectiveness. Personalized FL (PFL) (Kairouz et al., 2021) addresses this by customizing models to individual clients. *Personalized Fine-Tuning* (PFT) (Wu et al., 2022), a simple and practical strategy in the PFL family, is a widely adopted post-hoc, plug-and-play approach to diverse GFL methods. As shown in Fig. 1(a), PFT fine-tunes the final global model from GFL to personalize it. This simple strategy ensures easy implementation and adaptation across FL scenarios.

Unlike *process-integrated PFL* methods (*e.g.*, those involving server-client coordination that modifies the entire federated training process (Deng et al., 2020; Collins et al., 2021) or local training strategies that require iterative server feedback (Karimireddy et al., 2020; Tamirisa et al., 2024)), PFT eliminates the need for costly global-training-dependent adaptations. Instead, it fine-tunes the final GFL model once post-training, ensuring simplicity, broad compatibility, and deployment robustness without redesigning the GFL framework (see Tab. 1). These characteristics establish PFT as a critical fallback strategy when process-integrated PFL approaches prove infeasible — particularly in scenarios where global training protocols are unmodifiable due to infrastructure lock-in or legacy FL infrastructure, or strict coordination agreement constraints (*e.g.*, healthcare systems bound by long-term service agreements).

However, PFT often causes models to overfit on local data, thereby compromising the generalization of FL. This is particularly concerning in critical real-world applications, such as FL across multiple hospitals for disease diagnosis, where a local model must not only perform well on hospital patient data, but also generalize effectively to diverse patient populations that may be encountered on-site in the future (Xu et al., 2021). Therefore, balancing the optimization of individual client performance (personalization) with strong global performance (generalization across all clients) is crucial (Wu et al., 2022; Huang et al., 2024).

Table 1: Comparisons of Process-Integrated PFL vs. Post-Hoc PFT

Criterion	Process-Integrated PFL	PFT (Post-Hoc)
Global training modification	**Required** (aggregation changes or iterative local training with server feedback)	**None** (algorithm-agnostic)
Implementation Complexity	**High** (client-server coordination, custom aggregation/regularization)	**Low** (single fine-tuning step, client autonomy, plug-and-play)
Compatibility with GFL	**Limited** (framework-specific)	**Broad** (process-agnostic)

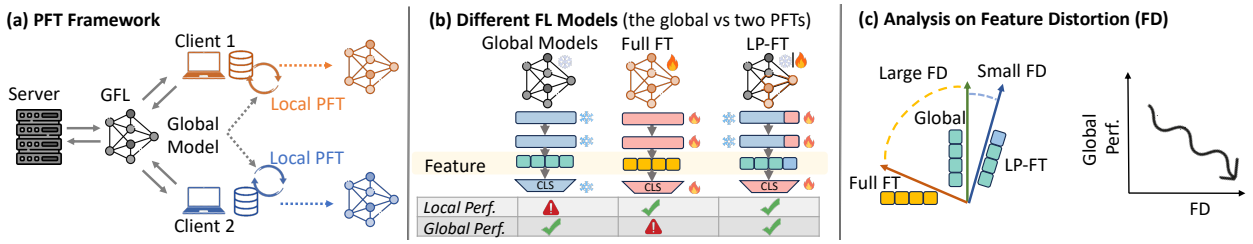

Figure 1: Overview of the problem setting and FL strategies investigated in this paper. (a) PFT framework, where each client fine-tunes a global model trained via GFL (e.g., FedAvg in this paper). Unlike process-integrated PFL, PFT focuses solely on the final fine-tuning stage with no further communication. (b) Three different FL models: the global FL model, the full-parameter FT (full FT) model, and the LP-FT model; their parameter updating patterns and local/global performance (perf.) under data heterogeneity; The fire icon indicates the actively tuned parameter, the frozen icon represents the fixed weight, and the mixed fire-frozen icon denotes the weight that is not actively tuned. (c) Visualization of feature distortion under PFL and its possible link to global generalization.

In this work, we conduct a comprehensive evaluation of various strategies for PFT in heterogeneous FL environments under different distribution shifts, categorized as covariate shift (Peng et al., 2019a; Hendrycks & Dietterich, 2019) and concept shift (Izmailov et al., 2022).

Despite meticulously tuning the hyper-parameters in some FT methods (full parameter FT, sparse FT Lee et al. (2018) and Proximal FT Li et al. (2020b)) adapted in FL, we observe persistent issues of local overfitting when increasing the local fine-tuning epochs, wherein localized performance gains are achieved at the significant cost of global generalization.

LP-FT (Kumar et al., 2022)—a two-phase fine-tuning strategy that first updates *only* the linear classifier (Linear Probing, LP) before optimizing all parameters (Full Fine-Tuning, FT)—has demonstrated state-of-the-art performance in centralized learning by mitigating overfitting and enhancing domain adaptation. However, its potential to address FL challenges, such as client data heterogeneity and instability during decentralized personalization, remains unexplored. In FL, local fine-tuning risks overfitting to client distributions and diverging from globally useful representations. LP-FT's structured separation of updating the head and then fine-tuning offers a principled framework to stabilize personalization in non-IID settings while preserving global knowledge.

Yet, no work has rigorously evaluated LP-FT's efficacy in FL—a critical oversight given the growing demand for lightweight, flexible, and robust personalization strategies. Empirically, we conduct a comprehensive evaluation across seven datasets and diverse distribution shifts, benchmarking our adapted LP-FT against other advanced fine-tuning methods in our PFT framework. Our findings reveal two key insights: (1) existing PFT methods suffer from personalized overfitting, where local fine-tuning distorts feature representations, degrading global performance (Fig. 2); (2) LP-FT mitigates this issue, preserving generalization while enhancing local adaptation under extreme data heterogeneity. Further, extensive ablation studies (Fig. 4) confirm that LP-FT reduces federated feature distortion, establishing it as a strong and scalable baseline for PFT in FL.

Theoretically, we revisit *feature distortion*–a key challenge previously defined in centralized LP-FT as feature shifts under out-of-domain fine-tuning—in FL's unique setting of partially overlapping local and global distributions. Unlike centralized analyses (Kumar et al., 2022), which assume a single ground-truth function, FL involves multiple client-specific ground-truth functions, necessitating a new theoretical framework. We address this by decoupling the feature extractor and classifier to analyze LP-FT's adaptation to heterogeneous client data. Further, we introduce a combined covariate-concept shift setting, better reflecting real-world FL scenarios. Our analysis reveals conditions under which LP-FT outperforms full fine-tuning, advancing the understanding of fine-tuning strategies in FL.

This paper takes a closer look at PFT and establishes LP-FT as a theoretically grounded and empirically viable solution for FL's unique constraints. In summary, our contributions are threefold: (1) Methodologically, this paper presents the first systematic and in-depth study on the post-hoc and plug-and-play PFT framework and introduces LP-FT as an effective approach for handling diverse distribution shifts. We comprehensively demonstrate its ability to balance personalization and generalization in the FL setting. (2) Empirically, we conduct extensive experiments across seven datasets under various distribution shifts, complemented by thorough ablation studies. Our results validate the robustness of LP-FT and reveal overfitting tendencies in prior PFT methods. These empirical insights not only establish LP-FT as a strong baseline for PFT but also provide a foundation for future research in simple and flexible FL personalization. (3) Theoretically, we offer a rigorous theoretical analysis of LP-FT using two-layer linear networks, demonstrating its superior ability to preserve global performance compared to FT in both concept shift and combined concept-covariate shift scenarios.

2 Related Work

Fine-Tuning pre-trained models has gained prominence in centralized learning, particularly with the rise of foundation models (Bommasani et al., 2021). However, fine-tuning with limited data often leads to overfitting. *Model soups* (Wortsman et al., 2022b) and partial fine-tuning (Lee et al., 2023) further enhance adaptation by selectively updating model components. LP-FT (Kumar et al., 2022), which combines linear probing with full fine-tuning, addresses feature distortions and provides insights into model adaptation under diverse shifts (Trivedi et al., 2023). However, the effectiveness of these centralized fine-tuning strategies in the heterogeneous FL setting remains largely underexplored.

Personalized FL aims to address the challenges of decentralized learning with non-IID data. Classical *general FL (GFL)* methods, such as FedAvg (McMahan et al., 2017), struggle in such settings. Despite the advancements in GFL methods (*e.g.*, FedNova (Wang et al., 2020)), FedProx (Li et al., 2020a), Scaffold (Karimireddy et al., 2020)), their focus on building a single global model does not adequately address the data heterogeneity inherent in FL, leading to the emergence of *personalized FL (PFL)* (Ghosh et al., 2020; Yu et al., 2020), which focuses on tailoring individualized models for each client. However, most PFL methods are *process-integrated*, requiring modifications to the global training pipeline through server-client coordination (Deng et al., 2020; Collins et al., 2021) or iterative local training with server feedback (Karimireddy et al., 2020; Tamirisa et al., 2024), or modifying training with customized clustering/regularization (Guo et al., 2024; Son et al., 2024). These approaches impose constraints on flexibility and deployment, as we summarized in Tab. 1. In contrast, *post-hoc personalized fine-tuning (PFT)* Wu et al. (2022) fine-tunes the final global model from GFL without modifying the training process, providing a lightweight and flexible approach for FL personalization. However, its potential is underexplored, possibly due to overfitting risks on client data. Additional discussion on personalization and fine-tuning is in App. B.

3 Empirical Study of PFT

To systematically investigate the challenges and opportunities in PFT, we present a comprehensive empirical study. First, in Sec. 3.1, we formalize the problem of PFT and characterize the spectrum of data heterogeneity to be studied. Next, Sec. 3.2 details our experimental setup, including datasets and PFT strategies under consideration. Our investigation then addresses a critical yet understudied phenomenon: Sec. 3.3 analyzes the prevalence of *personalized overfitting* in PFT across distribution shifts, even with careful hyper-parameter

tuning. Motivated by this finding, Sec. 3.4 introduces LP-FT and benchmarks its performance against alternative PFT strategies in FL, showing its superior ability to balance local adaptation with global knowledge retention. Finally, to uncover the mechanistic drivers of generalization challenges, Sec. 3.6 conducts the first systematic analysis of federated feature distortion—quantifying how client-specific fine-tuning trajectories alter latent representations and degrade model robustness.

3.1 Overview and Definitions

Problem Setting. In a FL setting, each client $i \in [C]$ has a local dataset $(\mathbf{X}_i, \mathbf{Y}_i)$ generated from a potentially distinct distribution, which may differ across clients due to distribution shifts. PFT aims to optimize local model parameters θ_L for each client, initialized from a well-trained global model θ_G. The objective is to minimize the local loss $\mathcal{L}_L(\theta_L)$ for improved local performance while ensuring that the global loss $\mathcal{L}_G(\theta_L)$ remains close to that of a pre-trained global model. This creates a trade-off between personalization (minimizing local loss) and maintaining generalization (minimizing global loss) across clients. The global data distribution $\mathcal{D}_G$ is defined as a mixture of the local distributions $\mathcal{D}_i$, given by $\mathcal{D}_G = \frac{1}{C}\sum_{i\in[C]} \mathcal{D}_i$.

We formally define distributions of interests, concept shift and covariate shift that directly lead to feature shift in heterogeneous FL context[1], following Li et al. (2021a).

Covariate Shift refers to variations in the input feature distribution across clients while keeping the conditional distribution of the output given the input consistent. Formally, for any pair of clients i and j with $i \neq j$, the data-generating process is characterized by:

$$P_i(x) \neq P_j(x), \quad \text{but} \quad P_i(y \mid x) = P_j(y \mid x) \quad \text{for all } i \neq j.$$

This means that while clients i and j may have different input distributions $P_i(x)$ and $P_j(x)$, the conditional distribution $P(y \mid x)$ remains consistent across all clients.

Concept Shift occurs when the conditional relationship between input features and outputs differs across clients, while the input feature distribution remains unchanged. Formally, for any two clients i and j with $i \neq j$, the data-generating process satisfies:

$$P_i(y \mid x) \neq P_j(y \mid x), \quad \text{but} \quad P_i(x) = P_j(x) \quad \text{for all } i \neq j.$$

This implies that although all clients share the same input distribution $P(x)$, the conditional distribution $P_i(y \mid x)$ varies, reflecting different mappings between features and labels across clients.

3.2 Empirical Analysis Settings

Datasets with Covariate Shift. We include `Digit5`, `DomainNet`, `CIFAR10-C`, and `CIFAR100-C`. `Digit5` and `DomainNet` belong to the *feature-shift* subgroup, where the data features represent different subpopulations within the same classes. For example, `Digit5` contains 10-digit images collected from various sources with different backgrounds, such as black-and-white for MNIST and colorful digits for synthetic datasets. `CIFAR10-C` and `CIFAR100-C` fall under the *input-level shift* category, where 50 types of image corruptions are introduced for evaluation. We simulate 50 clients, each corresponding to a specific corruption type, as detailed in previous works Hendrycks & Dietterich (2018); Mintun et al. (2021); Chen et al. (2021). A detailed explanation of the data splitting and its introduction is provided in Tab. 7 in Appendix. The visualizations of data are provided in Fig. 5.

Datasets with Concept Shift. `CheXpert` and `CelebA` are included for this part, whereas both belong to the *spurious correlation-based shift* subgroup, which involves misleading relationships in the training data that models may exploit, despite being unrelated to the actual target. This reliance can lead to poor performance when such correlations are absent in new data, classifying it as a form of concept shift (Izmailov et al., 2022). Similarly, Tab. 7 and Fig. 5 provide further details.

Fine-tuning Strategies. Our study focuses on post-hoc PFT, a plug-and-play framework that operates exclusively after GFL training. Unlike conventional fine-tuning in centralized settings that primarily addresses

[1]We also realized that LP-FT can be effective for label shift settings as the results shown in App. 3.5.

domain adaptation by transferring a model from a source to a disjoint target domain, PFT operates on a global model pre-trained via GFL, which has already been exposed to heterogeneous client data during collaborative training and must balance local performance (adapting to a client's unique distribution) with global performance (avoiding overfitting to statistically biased local updates and preserving cross-client generalizability).

In this study, we establish a suite of fine-tuning strategies that can be easily integrated into PFL as **baselines** for PFT: *Full-parameter FT* is a naive FT strategy. It adjusts all model parameters. *Proximal FT* (Li et al., 2020b) aims to preserve the pre-trained model's original knowledge. It applies proximal regularization to penalize large deviations from the initial model parameters, helping to maintain generalization. *Sparse FT* (Lee et al., 2018) promotes sparsity in parameter updates. It adjusts only the most relevant weights, enhancing efficiency while regularizing the training from overfitting. *Soup FT* (Wortsman et al., 2022a) improves robustness by averaging the weights of multiple fine-tuned model instances. Each instance is trained with different initializations, creating a "model soup" that integrates their strengths. *LSS FT* (Chen et al., 2024) (Local Superior Soups) is an innovative model interpolation-based local training technique designed to enhance FL generalization and communication efficiency by encouraging the exploration of a connected low-loss basin through optimizable and regularized model interpolation. Each strategy is designed to balance model performance with different priorities, such as preserving knowledge, enhancing robustness, or improving efficiency. A more detailed experiment setting is presented in App. C.[2]

3.3 Global and Local Performance Trends in PFT Baselines

In practice, PFT is susceptible to overfitting to local data, due to the relatively small amount of data available at local clients. Note that the *overfitting* defined in the FL context is characterized by *a consistent improvement in local performance while global performance noticeably deteriorates (Wu et al., 2022; Chen et al., 2023) – the average gain in local performance can be smaller than the loss in global performance.* To measure the model's overall local and global performance, we measure the averaged client-wise local and global accuracy. Specifically, this metric reflects the average performance between clients' *local* test accuracy and their local model's accuracy on the rest of the clients (*global* accuracy). The metric's decreasing trend with increasing local training epochs during the finetuning stage indicates personalized overfitting. Notably, this trend persists even when considering only global performance metrics, as local performance tends to show increases in PFT under overfitting conditions.

In all subplots of Fig. 2, we evaluate baseline PFT strategies under diverse distribution shifts, including input-level shifts (`CIFAR100-C`), feature-level shifts (`Digit5`), and spurious correlation-based shifts (`CheXpert`). We systematically adjusted hyperparameters to evaluate their impact on performance. Fig. 2a demonstrates that overfitting persists even when fine-tuning with reduced learning rates. Fig. 2b reveals that gradient sparsity adjustments (where higher sparsity rates mask more parameter updates) fail to mitigate overfitting as training epochs increase. Fig. 2c further shows that proximal regularization terms, designed to bias updates toward the initial global model, still exhibit global performance decay despite regularization.

3.4 Performance Comparison

Linear Probing then Fine-Tuning. To address the challenge of personalized overfitting in conventional fine-tuning methods within PFT, we propose a simple yet effective approach through Linear Probing followed by Fine-Tuning (LP-FT) for FL. The idea is motivated by LP-FT (Kumar et al., 2022)—a two-phase fine-tuning strategy in centralized training that first updates *only* the linear classifier (Linear Probing, LP) before optimizing all parameters (Full Fine-Tuning, FT) to improve out-of-domain performance while preserving in-domain performance. We adapt the strategy in PFT as follows: *In practice, clients initialize weights from the model after GFL, first perform linear probing, and then fine-tune the full model as shown in Fig. 1 (b).* This LP-FT approach achieves strong personalization while maintaining generalizability across diverse clients.

[2]We primarily focus on CNN-based models. We also include parameter-efficient fine-tuning results on transformer-based models in Appendix Tab. 8.

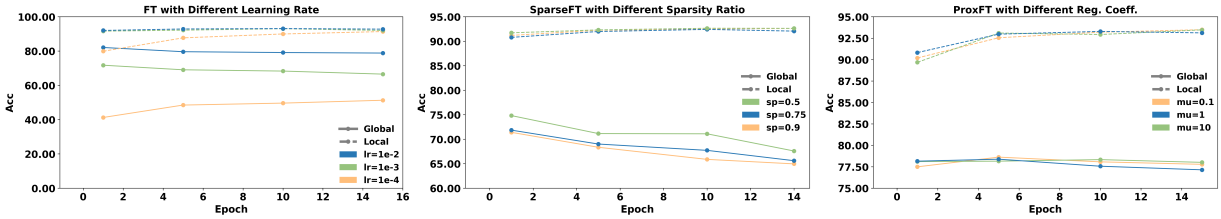

(a) **Full FT** (b) **Sparse FT** (c) **Proximal FT**

Figure 2: Visualization of the prevalence of personalization overfitting across different distribution shift scenarios, where (a) shows the global and local accuracy under different learning rates for full-parameter fine-tune; (b) shows the different sparsity rate for sparse fine-tune; (c) shows the different regularization strength under the proximal fine-tune. In all subfigures, the global accuracy is shown as the solid line, and the local accuracy is shown as the dashed line. As shown, global accuracy consistently declines while local accuracy either increases or remains stable across different hyperparameter settings. This suggests that PFT baseline methods are prone to overfitting, even with careful hyperparameter tuning.

Experimental Settings. To isolate the impact of PFT strategies and avoid conflating gains from GFL optimization, we standardize the GFL stage by fixing its method to FedAvg, the foundational and most widely used GFL method. Within this framework, we focus on comparing different *post-hoc* FT methods to demonstrate the effectiveness of LP-FT in PFT (see Fig. 1 (a)). After the GFL stage, all the clients further fine-tune the obtained global model using local data for 15 epochs for personalization. The final models are evaluated using the *metrics* described below. Details of the datasets, preprocessing steps, data splitting, and models used are provided in App. C.3, Tab. 7.

Metrics. We adapt five metrics in our baseline experiments: *(1) Local Accuracy (Local)* measures the performance of the PFT model on the client's local test set. Higher *Local Acc* indicates better personalization. *(2) Global Accuracy (Global)* measures the PFT model's average test accuracy over all other clients' test sets. Higher *Global Acc* indicates better generalization. *(3) Client-wise Standard Deviation (C-Std.)* calculates the standard deviation of local test accuracies across all clients. Lower *C-Std.* indicates less variance in performance among clients. *(4) Worst Accuracy (Worst)* reports the lowest test accuracy among all clients. The closer this value is to *Local Acc*, the better the worst-case generalization. *(5) Average* reports the average of both *Local Acc* and *Global Acc*, providing a better understanding of the tradeoff between personalization (local performance) and generalization (global performance). All metrics, except *C-Std.*, are averaged over the number of clients, and higher values are preferable. For *C-Std.*, lower values are better.

Results. Our results are presented in Tab. 2, where the best method is highlighted in **bold**. Datasets with the same distribution shift pattern are grouped into the same colors as detailed in the caption. Tab. 2 shows that LP-FT consistently achieves the highest global and average accuracy across most datasets, demonstrating strong generalization and personalization performances, particularly in challenging conditions like `CIFAR100-C` and `CIFAR10-C`. Sparse FT also performs well, especially in `Digits5` and `DomainNet`, but generally lags behind LP-FT. LSS FT, Soup FT and Proximal FT show mixed results, with stronger performance in specific datasets such as `CheXpert` but weaker overall compared to LP-FT. Standard fine-tuning consistently underperforms, highlighting the limitations of basic fine-tuning methods in heterogeneous data scenarios.

3.5 Label Shift

In this section, we examine the impact of LP-FT on the label shift scenario. We simulated label shift using a Dirichlet distribution with an alpha parameter set to 0.1. The dataset was distributed across 20 clients, and we trained a ResNet18 model for classification. Results is shown in Table 3.

Tab. 3 compares different fine-tuning methods on CIFAR10 across multiple evaluation metrics, including local performance, global performance, robustness to corruption (C-Std.), worst-case performance, and average performance. Among the methods, LP-FT achieves the best results, excelling in local performance (90.15), global evaluation (17.73), and average performance (35.96). Proximal FT and Sparse FT also perform

Table 2: Performance of various PFT strategies. **Red** represents the *input shift* subgroup; **green** from the *feature-shift* subgroup; **blue** the *spurious correlation-based shift* subgroup. Each experiment is performed three times independently with different random seeds, and the standard deviation of the results is presented in parentheses. ↑ indicates that higher values are better, while ↓ indicates that lower values are better.

Dataset	Method	Local ↑	Global ↑	C-Std. ↓	Worst ↑	Average ↑
CIFAR10-C	FT	54.50 (0.64)	44.16 (0.13)	**10.04 (0.06)**	19.83 (0.18)	39.50 (0.33)
	Proximal FT	61.76 (0.13)	53.58 (0.14)	11.61 (0.08)	25.82 (0.12)	47.05 (0.07)
	Soup FT	56.36 (0.23)	44.94 (0.06)	10.22 (0.06)	20.47 (0.35)	40.59 (0.09)
	Sparse FT	61.31 (0.01)	50.21 (0.17)	11.10 (0.11)	24.56 (0.09)	45.36 (0.04)
	LSS FT	56.21 (0.33)	46.81 (0.04)	10.05 (0.08)	21.61 (0.37)	43.67 (0.08)
	LP-FT	**63.55 (0.04)**	**55.35 (0.01)**	12.45 (0.01)	**26.33 (0.06)**	**48.41 (0.03)**
CIFAR100-C	FT	20.05 (0.05)	14.45 (0.04)	**5.37 (0.02)**	3.37 (0.06)	12.62 (0.03)
	Proximal FT	27.38 (0.15)	19.96 (0.11)	6.90 (0.04)	4.84 (0.04)	17.41 (0.05)
	Soup FT	20.99 (0.24)	14.81 (0.04)	5.48 (0.03)	3.56 (0.01)	13.12 (0.06)
	Sparse FT	28.93 (0.04)	20.66 (0.02)	7.75 (0.02)	5.05 (0.09)	18.15 (0.10)
	LSS FT	20.54 (0.19)	15.42 (0.03)	5.32 (0.03)	3.62 (0.01)	14.22 (0.06)
	LP-FT	**32.60 (0.14)**	**25.44 (0.10)**	9.66 (0.04)	**5.92 (0.06)**	**21.32 (0.04)**
Digit5	FT	91.17 (0.90)	67.87 (0.74)	22.93 (0.28)	42.03 (0.48)	67.02 (0.70)
	Proximal FT	**92.09 (0.18)**	81.40 (0.03)	15.04 (0.15)	61.71 (0.16)	78.40 (0.09)
	Soup FT	91.82 (0.34)	70.82 (0.43)	21.99 (0.67)	45.10 (1.27)	69.02 (0.65)
	Sparse FT	91.43 (0.31)	76.89 (0.72)	17.90 (0.38)	54.21 (0.56)	74.21 (0.35)
	LSS FT	91.59 (0.28)	73.13 (0.30)	22.04 (0.53)	45.32 (1.13)	71.15 (0.53)
	LP-FT	91.20 (0.04)	**82.78 (0.05)**	**13.75 (0.02)**	**65.80 (0.02)**	**79.92 (0.02)**
DomainNet	FT	64.90 (1.18)	42.48 (0.58)	17.49 (0.75)	22.31 (0.93)	43.23 (0.52)
	Proximal FT	67.20 (1.39)	56.05 (0.27)	**16.68 (0.36)**	33.20 (1.79)	52.60 (0.35)
	Soup FT	67.48 (0.61)	44.27 (0.46)	18.44 (0.42)	23.73 (1.24)	44.49 (0.54)
	Sparse FT	**69.62 (0.53)**	50.24 (0.44)	18.14 (0.17)	27.89 (0.15)	49.14 (0.45)
	LSS FT	66.37 (0.53)	45.34 (0.40)	18.02 (0.38)	22.63 (1.05)	45.75 (0.42)
	LP-FT	68.50 (0.19)	**57.52 (0.20)**	17.36 (0.21)	**34.53 (0.44)**	**53.52 (0.19)**
CheXpert	FT	76.18 (0.41)	76.25 (0.56)	0.35 (0.13)	76.31 (0.76)	76.25 (0.44)
	Proximal FT	76.44 (0.07)	76.63 (0.09)	0.71 (0.09)	76.81 (0.07)	76.63 (0.07)
	Soup FT	77.51 (0.15)	77.49 (0.31)	0.48 (0.07)	77.46 (0.43)	77.49 (0.26)
	Sparse FT	77.29 (0.13)	77.20 (0.14)	**0.31 (0.11)**	77.11 (0.25)	77.20 (0.14)
	LSS FT	77.49 (0.14)	77.51 (0.28)	0.52 (0.08)	**77.53 (0.37)**	77.52 (0.24)
	LP-FT	**77.64 (0.37)**	**77.54 (0.37)**	0.53 (0.41)	77.43 (0.71)	**77.54 (0.37)**
CelebA	FT	90.55 (1.20)	73.76 (2.15)	18.79 (3.64)	53.52 (5.51)	72.39 (2.84)
	Proximal FT	**93.74 (0.59)**	81.11 (0.82)	13.39 (1.14)	67.50 (2.10)	80.78 (0.90)
	Soup FT	89.42 (2.16)	75.28 (1.11)	16.29 (1.19)	57.79 (2.90)	74.17 (1.50)
	Sparse FT	91.43 (0.48)	77.32 (1.46)	14.16 (2.57)	62.94 (4.34)	77.65 (1.65)
	LSS FT	89.17 (2.05)	77.35 (1.03)	16.23 (1.28)	59.64 (2.86)	76.74 (1.46)
	LP-FT	93.24 (0.17)	**83.32 (0.31)**	**11.18 (0.14)**	**71.89 (0.75)**	**82.82 (0.64)**

competitively, with improvements over standard fine-tuning (FT) and Soup FT in most metrics. All methods show near-identical performance in the worst-case scenario (0.01), indicating a shared limitation in extreme cases. Overall, LP-FT demonstrates the most robust and effective fine-tuning approach on CIFAR10.

3.6 Insight and Explanation on the Observations

Given the unique design of LP-FT, we hypothesize that its superior performance in PFT stems from its ability to mitigate federated feature distortion — a phenomenon where client-specific fine-tuning disrupts the global model's learned representations. We empirically validate this hypothesis through a systematic analysis of feature space dynamics across diverse data heterogeneity scenarios.

	Baseline	Local	Global	C-Std.	Worst	Avg
CIFAR10	FT	87.20 (0.24)	16.67 (0.14)	**26.81 (1.47)**	0.01 (0.00)	34.62 (0.09)
	Proximal FT	89.80 (1.21)	17.42 (1.46)	27.31 (0.08)	0.01 (0.00)	35.75 (0.09)
	Soup FT	88.16 (0.15)	16.94 (0.05)	27.07 (0.11)	0.01 (0.00)	35.04 (0.04)
	Sparse FT	89.16 (0.00)	17.54 (0.14)	27.27 (0.02)	0.01 (0.00)	35.57 (0.04)
	LP-FT	**90.15 (0.43)**	**17.73 (0.16)**	27.37 (0.09)	0.01 (0.00)	**35.96 (0.10)**

Table 3: Comparison of PFT methods on CIFAR10 label shift setting.

Federated Feature Distortion. Consider a feature extraction function $f : \mathcal{X} \to \mathbb{R}^k$, which maps inputs from the input space $\mathcal{X}$ to a representation space $\mathbb{R}^k$. Let θ_G denote the global pre-trained model and θ_i the fine-tuned model after local fine-tuning for client i. Assume there are C clients in total, each with n samples. Let $x_{c,j}$ represent the j-th data point of the c-th client. The *federated feature distortion* $\Delta_c(f)$ quantifies the change in features after fine-tuning for the c-th client, defined as the average ℓ_2 distance between the representations produced by the global model and the locally fine-tuned model over all data points across all clients. Formally, it is expressed as: $\Delta_c(f) = \frac{1}{n}\sum_{j=1}^{n} \|f(\theta_G; x_{c,j}) - f(\theta_c; x_{c,j})\|_2$, where $\|\cdot\|_2$ is the ℓ_2 distance in the representation space $\mathbb{R}^k$. We compute the average of $\Delta_c(f)$ across all clients to represent the feature distortion in the PFT setting, as shown in Fig. 3.

Empirical Validation. To quantify federated feature distortion, we measure the ℓ_2 distance between global and locally fine-tuned feature representations using `DomainNet` and `Digit5`. As shown in Fig. 3(a), the full FT method induces severe feature distortion, correlating with a significant drop in global accuracy, whereas LP-FT maintains stable global performance with lower distortion.

To further isolate the effect of feature distortion from local loss magnitude, we apply loss flooding (Ishida et al., 2020) to control local training loss levels (0.1, 0.5, 1.0). Fig. 3(b) shows that at fixed local loss levels, LP-FT consistently outperforms FT in global accuracy, confirming that its advantage stems from reduced feature distortion rather than differences in local optimization dynamics.

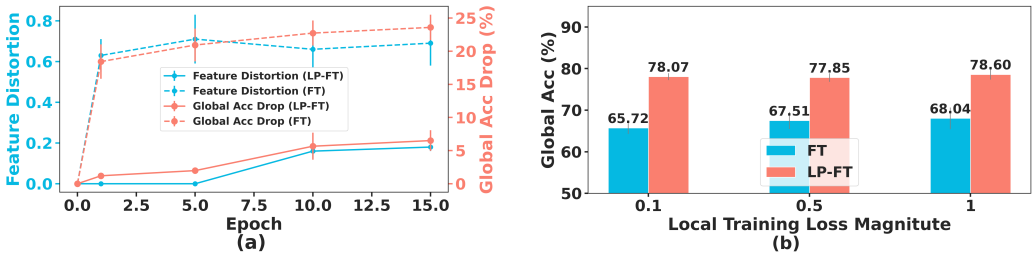

Figure 3: Observations of the feature distortion in PFT setting, where (a) presents the positive correlation between global performance drops and feature distortion intensity on `DomainNet` and (b) presents the ablation study on preserving federated features with controlled local train loss on `Digit5`. We set local loss thresholds (0.1, 0.5, and 1.0) and used gradient ascent when the loss fell below, ensuring training loss fluctuated around these points.

4 Theoretical Analysis of the LP-FT in FL

Building on our empirical observations in Sec. 3, where LP-FT consistently outperforms baseline PFT methods and demonstrates a significant reduction in federated feature distortion, we now present a theoretical analysis to uncover the mechanistic principles underlying its success. To understand how feature learning impacts generalization error in PFT, we decompose the data-generating function and the model into two components: a feature extractor and a linear head. This decomposition allows us to distinguish between the learned features and their influence on performance. Specifically, in Sec. 4.1 and Sec. 4.2, we formalize concept and covariate shifts within a two-layer linear network and examine how LP-FT effectively adapts to these shifts, outperforming full-parameter fine-tuning (FT) in FL.

Overview of Theoretical Analysis: To compare the performance of LP-FT and FT, we make assumptions about the data-generating function for clients (Assumption 4.1) and a specific model structure (Assumption 4.2). Based on these assumptions, we analyze the global performance of LP-FT and FT under concept shift (Theorem 4.4) and combined concept-covariate shift (Theorem 4.5).

4.1 LP-FT's Global Performance Under Concept Shift

In this section, we analyze LP-FT's performance compared to FT under concept shift. To facilitate a rigorous theoretical study, we define the data-generating process and model structure across clients, assuming both are represented by two-layer linear networks, as in (Kumar et al., 2022).

Assumption 4.1 (Data-Generating Process)**.** The data-generating function for client i is given by $y_i = {V_i^*}^T B_* x_i$ for all $i \in [C]$, where $y_i \in \mathbb{R}$, C is the number of clients, $x_i \in \mathbb{R}^d$, $B_* \in \mathbb{R}^{k \times d}$, and $V_i^* \in \mathbb{R}^k$. All clients share a common feature extractor B_*, assumed to have orthonormal rows, while their linear heads V_i^* differ. Each V_i^* decomposes as $V_i^* = \begin{bmatrix} {V_{com}^*}^T & \lambda e_i^T \end{bmatrix}^T$, where $V_{com}^* \in \mathbb{R}^m$ is shared across clients, $e_i \in \mathbb{R}^C$ is a unit vector, and λ controls heterogeneity. Here, $m + C = k$.

This assumption distinguishes between a shared and client-specific component in the data-generating functions, allowing analysis of both global and local performance of PFT methods after fine-tuning.

Assumption 4.2 (Model Structure)**.** The training model is a two-layer linear network defined as $y = V^T B x$, where $V \in \mathbb{R}^k$ is the linear head and $B \in \mathbb{R}^{k \times d}$ is the feature extractor. The dimensions of V and B match Assumption 4.1, allowing the model to learn both shared and client-specific data components.

In PFT settings, our objective is to evaluate the performance of a model on both global and local data. By local data, we refer to the data of a specific client undergoing fine-tuning (e.g., client i). The local and global losses are defined using the Mean Squared Error (MSE) as follows:

$$\mathcal{L}_L(V, B) = \mathbb{E}_{(x,y)\sim\mathcal{D}_i}\big[\frac{1}{2}(V^T B x - y)^2\big] = \mathbb{E}_{x\sim\mathcal{D}_i}\big[\frac{1}{2}\big(V^T B x - {V_i^*}^T B_* x\big)^2\big],$$
$$\mathcal{L}_G(V, B) = \mathbb{E}_{(x,y)\sim\mathcal{D}_G}\big[\frac{1}{2}(V^T B x - y)^2\big] = \frac{1}{C}\sum_{i\in[C]} \mathbb{E}_{x\sim\mathcal{D}_i}\big[\frac{1}{2}\big(V^T B x - {V_i^*}^T B_* x\big)^2\big].$$

Since this section focuses on concept shift, we assume all clients' data is drawn from similar distributions. Accordingly, we assume for every client $i \in [C]$, the input features satisfy $\mathbb{E}_{x\sim\mathcal{D}_i}[xx^T] = I_d$.

With the theoretical framework established by Assumptions 4.1 and 4.2, we compare the global performance of LP-FT and FT, highlighting cases where LP-FT outperforms FT. As demonstrated in Collins et al. (2022) FedAvg learns a shared data representation among clients if such a common representation exists. In a PFT setting, the initial model is trained on data from all clients to capture their shared components. Thus, we initialize the model parameters as $B_0 = B_*$ and $V_0 = \begin{bmatrix} {V_{com}^*}^T & \mathbf{0} \end{bmatrix}^T$. In LP-FT, a step of linear probing first updates V_0 using local data while keeping B_0 fixed, followed by full fine-tuning to update both V and B. In contrast, FT performs only the second step. The following lemma characterizes B after one gradient descent step in FT, forming the basis for our comparison.

Lemma 4.3. *Under Assumptions 4.1 and 4.2, and assuming that $\mathbb{E}_{x\sim\mathcal{D}_i}[xx^T] = I_d$ for all clients $i \in [C]$, let the initial parameters before starting FT be $B_0 = B_*$ and $V_0 = \begin{bmatrix} {V_{com}^*}^T & \mathbf{0} \end{bmatrix}^T$. Assume fine-tuning is performed locally on the data of the i-th client. Let B_{FT} denote the feature extractor matrix after a single gradient descent step (processing the entire dataset once) with learning rate η. If $(b_j^{FT})^T$ is the j-th row of B_{FT}, then:*

$$\mathbb{E}\Big[(b_j^{FT})^T\Big] = (b_j^*)^T + \eta\lambda(V_0)_j(b_{m+i}^*)^T,$$

where $(b_j^*)^T$ is the j-th row of B_* , and $(V_0)_j$ is the j-th element of V_0 for $j \in [k]$.

This lemma examines the impact of FT on the feature extractor B_{FT}, highlighting the deviations from the pre-trained matrix $B_0 = B_*$. Given that all clients share the same B_* in their labeling functions, substantial changes to the feature extractor can degrade global performance. Since the matrix B functions as the feature

extractor in our framework, significant feature distortion occurs when B_{FT} deviates considerably from B_*. Building on Lemma 4.3, Theorem 4.4 offers a comparative analysis of the global performance of LP-FT versus FT in the context of concept shift.

Theorem 4.4. *Under Assumptions 4.1 and 4.2, and assuming $\mathbb{E}_{x\sim\mathcal{D}_i}[xx^T] = I_d$ for all clients $i \in [C]$, let the initial model parameters be $B_0 = B_*$ and $V_0 = \begin{bmatrix} {V^*_{com}}^T & \mathbf{0} \end{bmatrix}^T$. Let B_{FT} and V_{FT} denote the parameters of the FT method after one gradient descent step (processing the entire dataset once). For LP-FT, let B_{LPFT} and V_{LPFT} denote the parameters after (i) linear probing, which optimizes V with B fixed at B_*, and (ii) one gradient descent step with learning rate η. Then:*

$$\mathcal{L}_G(V_{LPFT}, B_{LPFT}) \leq \mathcal{L}_G(V_{FT}, B_{FT}).$$

This theorem characterizes the global performance of LP-FT, suggesting that under concept shift, LP-FT achieves better performance on global data than FT. When starting from a model initialized to capture the shared feature extractor and linear head among clients, LP-FT is more effective in minimizing global loss, aligning with common FL scenarios where the initial model leverages shared client structure.

4.2 LP-FT's Global Performance under Combined Concept and Covariate Shifts

In the previous section, we assumed all clients' data came from the same distribution with $\mathbb{E}_{x\sim\mathcal{D}_i}[xx^T] = I_d$. However, this may not hold in many practical scenarios. To address this, we introduce covariate shift, where each client's data is generated as $x_i = e_i + \epsilon z$, with $z \sim \mathcal{N}(0, I)$, e_i as a client-specific shift, and ϵ controlling the noise level. This extension captures the non-iid nature of data among clients and provides a framework to model data heterogeneity. The model structure and data-generating assumptions remain consistent with Sec. 4.1. This section thus considers both concept and covariate shifts. Theorem 4.5 analyzes the impact of heterogeneity on the global performance of LP-FT and FT.

Theorem 4.5. *Under Assumptions 4.1 and 4.2, let each client's data be $x_i = e_i + \epsilon z$, where $z \sim \mathcal{N}(0, I)$ and e_i is a client-specific shift. Assume the initial parameters are $B_0 = B_*$ and $V_0 = \begin{bmatrix} {V^*_{com}}^T & \mathbf{0} \end{bmatrix}^T$. Let B_{FT}, V_{FT} be the FT parameters after one gradient descent step, and B_{LPFT}, V_{LPFT} be the LP-FT parameters after linear probing and one gradient descent step (with learning rate η). Then, there exists a threshold λ^* such that for all $\lambda \leq \lambda^*$:*

$$\mathcal{L}_G(V_{LPFT}, B_{LPFT}) \leq \mathcal{L}_G(V_{FT}, B_{FT}).$$

Remark 4.6. In Theorem 4.5, the parameter λ characterizes the level of heterogeneity among clients. The theorem shows that under both covariate and concept shifts, LP-FT outperforms FT in low heterogeneity settings ($\lambda \leq \lambda^*$), highlighting its advantage in maintaining generalization. To further reinforce the theoretical insights and cover more extensive settings, App. 5.1 provides extensive empirical validation, confirming the global superiority of LP-FT over FT under combined concept-covariate shifts. While the theoretical analysis in Theorem 4.5 focuses on the low heterogeneity regime, the experiments in App. 5.1 explore a broader range, including both high and low heterogeneity levels. Notably, LP-FT consistently outperforms FT across all heterogeneity regimes, aligning with our theoretical results in Sec. 4.2, particularly for deep neural networks in realistic PFT settings. These findings validate and extend our theoretical insights, demonstrating LP-FT's robustness and superiority in diverse distribution shift scenarios (see also App. F).

5 Further Empirical Validations for Theoretical Findings

Despite being based on simplified data and model assumptions, our theoretical results demonstrate significant practical relevance. In this section, we empirically validate the contributions in Sec. 4, exploring the performance implications of controllable heterogeneities in neural networks and datasets.

Experimental Settings. To validate the impact of λ in Theorem 4.5, we simulate a controllable concept shift setting on the `Digit5` dataset with label-flipping under PFT for both FT and LP-FT. For each client, a proportion of labels is randomly flipped, referred to as the flipping ratio. For example, class one is flipped with class two for the first client, and class two with class three for the second, using a randomized mechanism. A higher flipping ratio indicates greater heterogeneity λ. The settings align with prior studies: the model is

Table 4: Performance under label-flipping for FT and LP-FT across different label-flipping ratios (LF.R.).

Metric	**LF.R. 20%**	**LF.R. 30%**	**LF.R. 40%**	**LF.R. 50%**
FT Avg. ↑	67.73	60.04	58.27	60.06
LP-FT Avg. ↑	79.83	72.95	71.55	73.26
FT Global ↑	68.76	55.18	53.70	56.17
LP-FT Global ↑	83.08	72.75	69.89	72.32
FT Local ↑	91.32	91.12	90.84	91.88
LP-FT Local ↑	91.23	89.20	90.02	90.87

pre-trained within the FL framework and used to initialize both FT and LP-FT. This simulates the combined concept-covariate shift discussed in Sec. 4.2. Flipping labels reflects different labeling functions, where higher flipping rates indicate stronger concept shifts. The `Digit5` dataset also introduces covariate shift, as outlined in Sec. 3.2.

Results. As shown in Tab. 5, LP-FT consistently outperforms FT in global performance across various flipping ratios. This aligns with our theoretical results in Sec. 4.2, especially for deep neural networks under realistic PFT settings. The flipping rate controls concept shift heterogeneity, with higher rates indicating greater heterogeneity, while varying data distributions introduce covariate shift. These experiments simulate the combined concept-covariate shift, as analyzed in our framework. Notably, LP-FT outperforms FT in all heterogeneity levels, validating its advantage in both low and high heterogeneity regimes (larger flipping ratios).

5.1 Further Empirical Validations for Theoretical Findings

Table 5: Performance under label-flipping for FT and LP-FT across different label-flipping ratios (LF.R.).

Metric	**LF.R. 20%**	**LF.R. 30%**	**LF.R. 40%**	**LF.R. 50%**
FT Avg. ↑	67.73	60.04	58.27	60.06
LP-FT Avg. ↑	79.83	72.95	71.55	73.26
FT Global ↑	68.76	55.18	53.70	56.17
LP-FT Global ↑	83.08	72.75	69.89	72.32
FT Local ↑	91.32	91.12	90.84	91.88
LP-FT Local ↑	91.23	89.20	90.02	90.87

Despite being based on simplified data and model assumptions, our theoretical results demonstrate significant practical relevance. In this section, we empirically validate the contributions in Sec. 4, exploring the performance implications of controllable heterogeneities in neural networks and datasets.

Experimental Settings. To validate the impact of λ in Theorem 4.5, we simulate a controllable concept shift setting on the `Digit5` dataset with label-flipping under PFT for both FT and LP-FT. For each client, a proportion of labels is randomly flipped, referred to as the flipping ratio. For example, class one is flipped with class two for the first client, and class two with class three for the second, using a randomized mechanism. A higher flipping ratio indicates greater heterogeneity λ. The settings align with prior studies: the model is pre-trained within the FL framework and used to initialize both FT and LP-FT. This simulates the combined concept-covariate shift discussed in Sec. 4.2. Flipping labels reflects different labeling functions, where higher flipping rates indicate stronger concept shifts. The `Digit5` dataset also introduces covariate shift, as outlined in Sec. 3.2.

Results. As shown in Tab. 5, LP-FT consistently outperforms FT in global performance across various flipping ratios. This aligns with our theoretical results in Sec. 4.2, especially for deep neural networks under realistic PFT settings. The flipping rate controls concept shift heterogeneity, with higher rates indicating greater heterogeneity, while varying data distributions introduce covariate shift. These experiments simulate the combined concept-covariate shift, as analyzed in our framework. Notably, LP-FT outperforms FT in all heterogeneity levels, validating its advantage in both low and high heterogeneity regimes (larger flipping ratios).

6 Conclusion

In this work, we studied an important PFL paradigm – PFT and tackled its key challenge of balancing local personalization and global generalization. We establish LP-FT as a theoretically grounded and empirically robust solution for PFT. Our work demonstrates that LP-FT effectively mitigates federated feature distortion, balancing client-specific adaptation with global generalization under extreme data heterogeneity. Methodologically, we are the first to adapt LP-FT to post-hoc PFT; empirically, we validate LP-FT's superiority across seven datasets; theoretically, we formalize its advantages in FL's unique covariate-concept shift regime. This work advances lightweight, deployable personalization for real-world FL systems.

Bibliography

Rishi Bommasani, Drew A. Hudson, Ehsan Adeli, Russ B. Altman, Simran Arora, Sydney von Arx, Michael S. Bernstein, Jeannette Bohg, Antoine Bosselut, Emma Brunskill, Erik Brynjolfsson, Shyamal Buch, Dallas Card, Rodrigo Castellon, Niladri S. Chatterji, Annie S. Chen, Kathleen Creel, Jared Quincy Davis, Dorottya Demszky, Chris Donahue, Moussa Doumbouya, Esin Durmus, Stefano Ermon, John Etchemendy, Kawin Ethayarajh, Li Fei-Fei, Chelsea Finn, Trevor Gale, Lauren Gillespie, Karan Goel, Noah D. Goodman, Shelby Grossman, Neel Guha, Tatsunori Hashimoto, Peter Henderson, John Hewitt, Daniel E. Ho, Jenny Hong, Kyle Hsu, Jing Huang, Thomas Icard, Saahil Jain, Dan Jurafsky, Pratyusha Kalluri, Siddharth Karamcheti, Geoff Keeling, Fereshte Khani, Omar Khattab, Pang Wei Koh, Mark S. Krass, Ranjay Krishna, Rohith Kuditipudi, and et al. On the opportunities and risks of foundation models. *CoRR*, abs/2108.07258, 2021.

Minghui Chen, Zhiqiang Wang, and Feng Zheng. Benchmarks for corruption invariant person re-identification. *arXiv preprint arXiv:2111.00880*, 2021.

Minghui Chen, Meirui Jiang, Qi Dou, Zehua Wang, and Xiaoxiao Li. Fedsoup: Improving generalization and personalization in federated learning via selective model interpolation. In *MICCAI (2)*, volume 14221 of *Lecture Notes in Computer Science*, pp. 318–328. Springer, 2023.

Minghui Chen, Meirui Jiang, Xin Zhang, Qi Dou, Zehua Wang, and Xiaoxiao Li. Local superior soups: A catalyst for model merging in cross-silo federated learning. *CoRR*, abs/2410.23660, 2024.

Liam Collins, Hamed Hassani, Aryan Mokhtari, and Sanjay Shakkottai. Exploiting shared representations for personalized federated learning. In *ICML*, volume 139 of *Proceedings of Machine Learning Research*, pp. 2089–2099. PMLR, 2021.

Liam Collins, Hamed Hassani, Aryan Mokhtari, and Sanjay Shakkottai. Fedavg with fine tuning: Local updates lead to representation learning. *Advances in Neural Information Processing Systems*, 35:10572–10586, 2022.

Yuyang Deng, Mohammad Mahdi Kamani, and Mehrdad Mahdavi. Adaptive personalized federated learning. *CoRR*, abs/2003.13461, 2020.

Yuyang Deng, Mohammad Mahdi Kamani, and Mehrdad Mahdavi. Distributionally robust federated averaging. *CoRR*, abs/2102.12660, 2021.

Pierre Foret, Ariel Kleiner, Hossein Mobahi, and Behnam Neyshabur. Sharpness-aware minimization for efficiently improving generalization. In *ICLR*. OpenReview.net, 2021.

Avishek Ghosh, Jichan Chung, Dong Yin, and Kannan Ramchandran. An efficient framework for clustered federated learning. In *NeurIPS*, 2020.

Yongxin Guo, Xiaoying Tang, and Tao Lin. Fedrc: Tackling diverse distribution shifts challenge in federated learning by robust clustering. In *ICML*. OpenReview.net, 2024.

Dan Hendrycks and Thomas G Dietterich. Benchmarking neural network robustness to common corruptions and surface variations. *arXiv preprint arXiv:1807.01697*, 2018.

Dan Hendrycks and Thomas G. Dietterich. Benchmarking neural network robustness to common corruptions and perturbations. In *ICLR (Poster)*. OpenReview.net, 2019.

Neil Houlsby, Andrei Giurgiu, Stanislaw Jastrzebski, Bruna Morrone, Quentin de Laroussilhe, Andrea Gesmundo, Mona Attariyan, and Sylvain Gelly. Parameter-efficient transfer learning for NLP. In *ICML*, volume 97 of *Proceedings of Machine Learning Research*, pp. 2790–2799. PMLR, 2019.

Edward J. Hu, Yelong Shen, Phillip Wallis, Zeyuan Allen-Zhu, Yuanzhi Li, Shean Wang, Lu Wang, and Weizhu Chen. Lora: Low-rank adaptation of large language models. In *ICLR*. OpenReview.net, 2022.

Chun-Yin Huang, Ruinan Jin, Can Zhao, Daguang Xu, and Xiaoxiao Li. Federated virtual learning on heterogeneous data with local-global distillation. *CoRR*, abs/2303.02278, 2023. doi: 10.48550/ARXIV.2303.02278. URL `https://doi.org/10.48550/arXiv.2303.02278`.

Chun-Yin Huang, Kartik Srinivas, Xin Zhang, and Xiaoxiao Li. Overcoming data and model heterogeneities in decentralized federated learning via synthetic anchors, 2024. URL `https://openreview.net/forum?id=PcBJ4pA6bF`.

Jeremy Irvin, Pranav Rajpurkar, Michael Ko, Yifan Yu, Silviana Ciurea-Ilcus, Chris Chute, Henrik Marklund, Behzad Haghgoo, Robyn Ball, Katie Shpanskaya, et al. Chexpert: A large chest radiograph dataset with uncertainty labels and expert comparison. In *Proceedings of the AAAI conference on artificial intelligence*, volume 33, pp. 590–597, 2019.

Takashi Ishida, Ikko Yamane, Tomoya Sakai, Gang Niu, and Masashi Sugiyama. Do we need zero training loss after achieving zero training error? In *ICML*, volume 119 of *Proceedings of Machine Learning Research*, pp. 4604–4614. PMLR, 2020.

Pavel Izmailov, Dmitrii Podoprikhin, Timur Garipov, Dmitry P. Vetrov, and Andrew Gordon Wilson. Averaging weights leads to wider optima and better generalization. In *UAI*, pp. 876–885. AUAI Press, 2018.

Pavel Izmailov, Polina Kirichenko, Nate Gruver, and Andrew Gordon Wilson. On feature learning in the presence of spurious correlations. In *NeurIPS*, 2022.

Ruinan Jin, Wenlong Deng, Minghui Chen, and Xiaoxiao Li. Debiased noise editing on foundation models for fair medical image classification. In *International Conference on Medical Image Computing and Computer-Assisted Intervention*, pp. 164–174. Springer, 2024.

Jean Kaddour, Linqing Liu, Ricardo Silva, and Matt J. Kusner. When do flat minima optimizers work? In *NeurIPS*, 2022.

Peter Kairouz, H. Brendan McMahan, Brendan Avent, Aurélien Bellet, Mehdi Bennis, Arjun Nitin Bhagoji, Kallista A. Bonawitz, Zachary Charles, Graham Cormode, Rachel Cummings, Rafael G. L. D'Oliveira, Hubert Eichner, Salim El Rouayheb, David Evans, Josh Gardner, Zachary Garrett, Adrià Gascón, Badih Ghazi, Phillip B. Gibbons, Marco Gruteser, Zaïd Harchaoui, Chaoyang He, Lie He, Zhouyuan Huo, Ben Hutchinson, Justin Hsu, Martin Jaggi, Tara Javidi, Gauri Joshi, Mikhail Khodak, Jakub Konečný, Aleksandra Korolova, Farinaz Koushanfar, Sanmi Koyejo, Tancrède Lepoint, Yang Liu, Prateek Mittal, Mehryar Mohri, Richard Nock, Ayfer Özgür, Rasmus Pagh, Hang Qi, Daniel Ramage, Ramesh Raskar, Mariana Raykova, Dawn Song, Weikang Song, Sebastian U. Stich, Ziteng Sun, Ananda Theertha Suresh, Florian Tramèr, Praneeth Vepakomma, Jianyu Wang, Li Xiong, Zheng Xu, Qiang Yang, Felix X. Yu, Han Yu, and Sen Zhao. Advances and open problems in federated learning. *Found. Trends Mach. Learn.*, 14 (1-2):1–210, 2021.

Sai Praneeth Karimireddy, Satyen Kale, Mehryar Mohri, Sashank J. Reddi, Sebastian U. Stich, and Ananda Theertha Suresh. SCAFFOLD: stochastic controlled averaging for federated learning. In *ICML*, volume 119 of *Proceedings of Machine Learning Research*, pp. 5132–5143. PMLR, 2020.

Alex Krizhevsky, Geoffrey Hinton, et al. Learning multiple layers of features from tiny images. *corr*, 2009.

Ananya Kumar, Aditi Raghunathan, Robbie Matthew Jones, Tengyu Ma, and Percy Liang. Fine-tuning can distort pretrained features and underperform out-of-distribution. In *ICLR*. OpenReview.net, 2022.

Namhoon Lee, Thalaiyasingam Ajanthan, and Philip HS Torr. Snip: Single-shot network pruning based on connection sensitivity. *arXiv preprint arXiv:1810.02340*, 2018.

Yoonho Lee, Annie S. Chen, Fahim Tajwar, Ananya Kumar, Huaxiu Yao, Percy Liang, and Chelsea Finn. Surgical fine-tuning improves adaptation to distribution shifts. In *ICLR*. OpenReview.net, 2023.

Hao Li, Zheng Xu, Gavin Taylor, Christoph Studer, and Tom Goldstein. Visualizing the loss landscape of neural nets. In *NeurIPS*, pp. 6391–6401, 2018.

Tian Li, Anit Kumar Sahu, Manzil Zaheer, Maziar Sanjabi, Ameet Talwalkar, and Virginia Smith. Federated optimization in heterogeneous networks. In *MLSys*. mlsys.org, 2020a.

Tian Li, Anit Kumar Sahu, Manzil Zaheer, Maziar Sanjabi, Ameet Talwalkar, and Virginia Smith. Federated optimization in heterogeneous networks. *Proceedings of Machine learning and systems*, 2:429–450, 2020b.

Xiaoxiao Li, Meirui Jiang, Xiaofei Zhang, Michael Kamp, and Qi Dou. Fedbn: Federated learning on non-iid features via local batch normalization. In *ICLR*. OpenReview.net, 2021a.

Xiaoxiao Li, Meirui Jiang, Xiaofei Zhang, Michael Kamp, and Qi Dou. Fedbn: Federated learning on non-iid features via local batch normalization. *arXiv preprint arXiv:2102.07623*, 2021b.

Ziwei Liu, Ping Luo, Xiaogang Wang, and Xiaoou Tang. Deep learning face attributes in the wild. In *Proceedings of International Conference on Computer Vision (ICCV)*, December 2015.

Yishay Mansour, Mehryar Mohri, Jae Ro, and Ananda Theertha Suresh. Three approaches for personalization with applications to federated learning. *CoRR*, abs/2002.10619, 2020.

Brendan McMahan, Eider Moore, Daniel Ramage, Seth Hampson, and Blaise Agüera y Arcas. Communication-efficient learning of deep networks from decentralized data. In *AISTATS*, volume 54 of *Proceedings of Machine Learning Research*, pp. 1273–1282. PMLR, 2017.

Eric Mintun, Alexander Kirillov, and Saining Xie. On interaction between augmentations and corruptions in natural corruption robustness. *Advances in Neural Information Processing Systems*, 34:3571–3583, 2021.

Xingchao Peng, Qinxun Bai, Xide Xia, Zijun Huang, Kate Saenko, and Bo Wang. Moment matching for multi-source domain adaptation. In *ICCV*, pp. 1406–1415. IEEE, 2019a.

Xingchao Peng, Qinxun Bai, Xide Xia, Zijun Huang, Kate Saenko, and Bo Wang. Moment matching for multi-source domain adaptation. In *Proceedings of the IEEE/CVF international conference on computer vision*, pp. 1406–1415, 2019b.

Ha Min Son, Moon-Hyun Kim, Tai-Myoung Chung, Chao Huang, and Xin Liu. Feduv: Uniformity and variance for heterogeneous federated learning. In *CVPR*, pp. 5863–5872. IEEE, 2024.

Rishub Tamirisa, Chulin Xie, Wenxuan Bao, Andy Zhou, Ron Arel, and Aviv Shamsian. Fedselect: Personalized federated learning with customized selection of parameters for fine-tuning. In *CVPR*, pp. 23985–23994. IEEE, 2024.

Puja Trivedi, Danai Koutra, and Jayaraman J. Thiagarajan. A closer look at model adaptation using feature distortion and simplicity bias. In *ICLR*. OpenReview.net, 2023.

Tiffany J. Vlaar and Jonathan Frankle. What can linear interpolation of neural network loss landscapes tell us? In *ICML*, volume 162 of *Proceedings of Machine Learning Research*, pp. 22325–22341. PMLR, 2022.

Jianyu Wang, Qinghua Liu, Hao Liang, Gauri Joshi, and H. Vincent Poor. Tackling the objective inconsistency problem in heterogeneous federated optimization. In *NeurIPS*, 2020.

Mitchell Wortsman, Gabriel Ilharco, Samir Ya Gadre, Rebecca Roelofs, Raphael Gontijo-Lopes, Ari S Morcos, Hongseok Namkoong, Ali Farhadi, Yair Carmon, Simon Kornblith, et al. Model soups: averaging weights of multiple fine-tuned models improves accuracy without increasing inference time. In *International conference on machine learning*, pp. 23965–23998. PMLR, 2022a.

Mitchell Wortsman, Gabriel Ilharco, Samir Yitzhak Gadre, Rebecca Roelofs, Raphael Gontijo Lopes, Ari S. Morcos, Hongseok Namkoong, Ali Farhadi, Yair Carmon, Simon Kornblith, and Ludwig Schmidt. Model soups: averaging weights of multiple fine-tuned models improves accuracy without increasing inference time. In *ICML*, volume 162 of *Proceedings of Machine Learning Research*, pp. 23965–23998. PMLR, 2022b.

Shanshan Wu, Tian Li, Zachary Charles, Yu Xiao, Ken Ziyu Liu, Zheng Xu, and Virginia Smith. Motley: Benchmarking heterogeneity and personalization in federated learning. *CoRR*, abs/2206.09262, 2022.

Jie Xu, Benjamin S. Glicksberg, Chang Su, Peter B. Walker, Jiang Bian, and Fei Wang. Federated learning for healthcare informatics. *J. Heal. Informatics Res.*, 5(1):1–19, 2021.

Tao Yu, Eugene Bagdasaryan, and Vitaly Shmatikov. Salvaging federated learning by local adaptation. *CoRR*, abs/2002.04758, 2020.

Contents

1 Introduction **1**

2 Related Work **3**

3 Empirical Study of PFT **3**
3.1 Overview and Definitions . . . 4
3.2 Empirical Analysis Settings . . . 4
3.3 Global and Local Performance Trends in PFT Baselines . . . 5
3.4 Performance Comparison . . . 5
3.5 Label Shift . . . 6
3.6 Insight and Explanation on the Observations . . . 7

4 Theoretical Analysis of the LP-FT in FL **8**
4.1 LP-FT's Global Performance Under Concept Shift . . . 9
4.2 LP-FT's Global Performance under Combined Concept and Covariate Shifts . . . 10

5 Further Empirical Validations for Theoretical Findings **10**
5.1 Further Empirical Validations for Theoretical Findings . . . 11

6 Conclusion **12**

Bibliography **12**

Contents **16**

A Related Work: Personalized Federated Learning and Fine-Tuning **17**

B Different Variants of Fine-tune Strategy **18**
B.1 Proximal FT . . . 18
B.2 Soup FT . . . 18
B.3 Sparse FT . . . 19
B.4 LSS FT . . . 19
B.5 LP-FT . . . 19

C Experimental Details **19**
C.1 Computing Environment and Hyper-parameters . . . 19
C.2 Visualization of Original Images . . . 19
C.3 Detailed Dataset and Model Information . . . 20

D Further Empirical Results **20**
D.1 Other PEFT Methods Distort Federated Feature . . . 20

E Proofs **23**

F Empirical Performance of LP-FT and FT Under Theorem 4.5 Conditions **32**

G Computational Overhead of LP-FT Relative to FT **33**

Roadmap of Appendix. This appendix provides all supplemental material referred to in the main paper. First, in Section A we review related work on personalized federated learning (FL) and fine-tuning. Section B introduces the variants of fine-tuning strategies evaluated in our experiments, including Proximal FT, Soup FT, Sparse FT, LSS FT, and LP-FT. Section C gives full experimental details: computing environment, hyperparameters, dataset visualizations (Fig. 5), and dataset/model statistics (Table 7). In Section D we present additional empirical results, including PEFT distortions (Table 8) and label-shift experiments (Table 3). Section B.1 contains full proofs of Lemma 4.3, Theorems 4.4 and 4.5, along with illustrative plots (Fig. 6). Finally, Section G analyzes the computational overhead of LP-FT vs. FT.

Table 6: Important notations used in the appendix

Notation	**Description**
C	Number of clients in federated learning
m	Dimension of the common part of the linear head shared across clients
d	Dimension of feature representations
k	Dimension of the linear head
$B \in \mathbb{R}^{k \times d}$	Feature extractor matrix
$B_* \in \mathbb{R}^{k \times d}$	Ground-truth feature extractor matrix (with orthonormal rows)
$V \in \mathbb{R}^k$	Linear head weight vector
$V_i^* \in \mathbb{R}^k$	Ground-truth linear head for client i
$V_0 \in \mathbb{R}^k$	Initial linear head before fine-tuning
$V_{\text{com}}^* \in \mathbb{R}^m$	Common component of linear heads across clients
λ	Concept shift magnitude (heterogeneity parameter)
ϵ	Noise scale in the covariate shift model
$\mathcal{D}_i$	Data distribution of client i
$\mathcal{D}_G$	Mixture of all clients' data distributions (global distribution)
η	Learning rate used during fine-tuning
θ_L	Parameters of the local model
θ_G	Parameters of the global model
$\mathcal{L}_L$	Local loss function
$\widehat{\mathcal{L}}_L$	Empirical local loss
$\mathcal{L}_G$	Global loss function

A Related Work: Personalized Federated Learning and Fine-Tuning

Personalized FL. Heterogeneous FL refers to a decentralized training paradigm that accommodates diverse and disparate data sources or devices participating in a collaborative model-building process. Examples include FedAvg (McMahan et al., 2017) and various improvements in terms of aggregation optimization and local optimization. It is shown to experience challenges in heterogeneous scenarios. Thus, various literature proposes alternative strategies. Here, we summarize these strategies into aggregation optimization and local optimization. FedNova (Wang et al., 2020) belongs to the category of Aggregation optimization, which normalizes and scales the local updates. Examples of local optimization include FedProx (Li et al., 2020a) and Scaffold (Karimireddy et al., 2020), where FedProx adds a L_2 regularization for each client and Scaffold adds a variance reduction term. However, these methods often exhibit limited personalization capabilities and may not adequately meet the performance requirements of different clients. Consequently, various personalized FL approaches have been proposed, with a primary emphasis on enhancing local client performance to the greatest extent possible. We can group these personalized FL strategies into clustering-based methods (Ghosh et al., 2020), transfer learning (Yu et al., 2020), and interpolating the local and global models (Mansour et al., 2020; Deng et al., 2021). Some FL methods (Guo et al., 2024; Son et al., 2024) highlight that existing federated learning methods often fail under feature shift despite addressing label shift, proposing clustering and regularization strategies respectively to tackle diverse distribution shifts in non-IID data settings.

Fine-Tuning. Fine-tuning pre-trained models has become increasingly popular with the rise of foundation models (Bommasani et al., 2021). However, fine-tuning with limited data often lead to overfitting. Several strategies can mitigate this issue, such as using optimizers that promote a flatter loss landscape (Li et al., 2018; Kaddour et al., 2022). Notably, Sharpness-Aware Minimization (SAM) (Foret et al., 2021) and Stochastic Weight Averaging (SWA) (Izmailov et al., 2018) are two popular methods that help achieve this. Additionally, a technique called *model soups* (Wortsman et al., 2022b), uses a simple greedy weight averaging approach similar to SWA, shown significant improvements in fine-tuning. An interesting perspective focuses on minimizing the linear mode connectivity barrier between the pre-trained and fine-tuned models, helping maintain consistency in decision-making mechanisms from a loss landscape perspective (Vlaar & Frankle, 2022). *Partial fine-tuning* is another common method to prevent overfitting, which involves selectively fine-tuning specific layers of the model to better adapt to variations in data distribution (Lee et al., 2023). Recent studies have introduced the concept of LP-FT (Kumar et al., 2022), highlighting potential distortions in pre-trained features and their underperformance in scenarios involving previously unseen data. Further research on LP-FT provides a deeper analysis of model adaptation (Trivedi et al., 2023), focusing on feature distortion and simplicity bias, thereby enhancing our understanding of fine-tuning mechanisms and safe model adaptation.

B Different Variants of Fine-tune Strategy

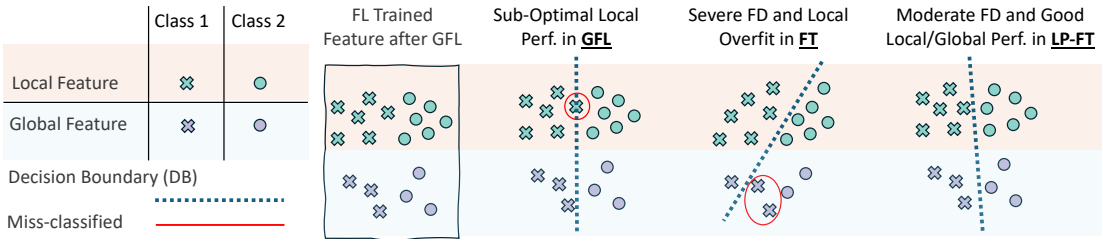

Figure 4: Illustration of federated feature distortion (FD) and decision boundaries.

This section provides an overview of the baseline techniques utilized in our study. We describe the characteristics and implementation specifics of three main fine-tuning methods: Proximal FT, Soup FT, and Sparse FT.

B.1 Proximal FT

Proximal Fine-Tuning (Proximal FT) (Li et al., 2020b) is a method that emphasizes preserving the original knowledge of the pre-trained model while adapting it to new tasks. This technique employs proximal regularization, which penalizes large deviations from the initial model parameters during the fine-tuning process. The primary advantage of Proximal FT is its ability to maintain the generalization capabilities of the pre-trained model, thus reducing the risk of overfitting to the new task's data. In our experiments, we used an L2 regularization term to enforce proximity between the pre-trained and fine-tuned weights, with a regularization coefficient of 0.01.

B.2 Soup FT

Soup Fine-Tuning (Soup FT) (Wortsman et al., 2022a) is an innovative approach that leverages the concept of "model soups," where multiple fine-tuned models are combined to create a more robust final model. The key idea is to fine-tune several instances of the pre-trained model on the target task with different random initializations or data shuffling, and then average the resulting weights to form a "soup." This method aims to enhance model robustness and performance by integrating the strengths of various fine-tuning instances. For our implementation, we fine-tuned five versions of the pre-trained model and averaged their parameters to create the final Soup FT model.

B.3 Sparse FT

Sparse Fine-Tuning (Sparse FT) (Lee et al., 2018) introduces sparsity constraints into the fine-tuning process, encouraging the model to update only a subset of its parameters. This approach aims to improve model efficiency and interpretability by ensuring that only the most relevant weights are adjusted during training. Sparse FT can be particularly beneficial for deploying models in resource-constrained environments where computational efficiency is paramount. In our experiments, we applied a gradient-based metric to the parameter prune, setting the regularization coefficient to 0.001 to achieve a balance between performance and sparsity.

B.4 LSS FT

In the context of FL, the Local Superior Soups (LSS) methodology (Chen et al., 2024) introduces a novel approach to enhance both generalization and communication efficiency. By leveraging model interpolation-based local training, LSS encourages clients to explore a connected low-loss basin through optimizable and regularized model interpolation. This strategy not only mitigates the challenges posed by data heterogeneity but also significantly reduces the number of communication rounds required for model convergence. Empirical evaluations have demonstrated the effectiveness of LSS across various widely used FL datasets, underscoring its potential as a catalyst for the seamless adaptation of pre-trained models in federated settings. In our experiments, we fine-tuned three candidate models for model interpolation and averaged their parameters to create the final Soup FT model.

B.5 LP-FT

Linear Probing and then Fine-Tuning (LP-FT) (Kumar et al., 2022) is a two-step transfer learning approach designed to balance in-distribution (ID) and out-of-distribution (OOD) performance. In the first step, linear probing trains only the final layer (head) while freezing the pretrained feature extractor to ensure OOD robustness. The second step fine-tunes all model parameters to improve ID accuracy while retaining the benefits of linear probing for OOD generalization. LP-FT addresses the trade-offs inherent in full fine-tuning by initializing with a well-aligned linear head, reducing feature distortion during optimization. Empirically, LP-FT demonstrates superior ID and OOD accuracy across diverse datasets.

C Experimental Details

C.1 Computing Environment and Hyper-parameters

All experiments in this paper are conducted on NVIDIA A40 Graphics cards using PyTorch. The Adam optimizer is employed with a learning rate of 1×10^{-3}. In FL for all datasets, the standard local model update epochs are set to 1. The communication round is set to be 100 epochs, where we validated the model results from FL converged. Unless specified otherwise, the batch size for all benchmarks is standardized at 128. To ensure a fair comparison with various baselines, all methods initiate the FL personalized fine-tuning with models derived from the best-performing global model in terms of overall effectiveness.

C.2 Visualization of Original Images

Datasets and Distribution Shifts. Figure 5 gives an overview of the benchmarks used in this study, organized by the four types of distribution shift we investigate—*feature-, input-, output-,* and *label-level.* All datasets are chosen to mirror the heterogeneity observed in real-world federated learning (FL) deployments.

- **Feature-level shift: Digit5 and DomainNet. Digit5** merges five digit domains—MNIST, SVHN, USPS, SynthDigits, and MNIST-M—whose diverse styles (e.g. grayscale scans vs. synthetic colors) induce substantial feature variations. **DomainNet** depicts everyday objects across six artistic domains (clip art, sketch, photo, *etc.*), further stressing the model's ability to transfer features across drastically different visual styles.

- **Input-level shift: CIFAR10-C and CIFAR100-C.** CIFAR10-C/100-C apply 50 corruption types (Gaussian noise, motion blur, pixelation, brightness, contrast, ...) to the original CIFAR images, emulating degradations caused by hardware or environment. These pixel-level perturbations leave semantics intact while challenging a model's robustness to distorted inputs—crucial for FL settings such as mobile sensing and autonomous driving.
- **Output-level shift: CheXpert and CelebA.** In **CheXpert**, we focus on two labels (Edema, No Finding) and partition clients to introduce demographic biases (e.g. male patients predominating in Edema, female in No Finding). **CelebA** clients are built by correlating gender and hair-color attributes (e.g. "blonde-haired females" vs. "non-blonde males"), yielding skewed label distributions that test a model's resilience to demographic imbalance.
- **Label-level shift: CIFAR10 (Dirichlet-α=0.1).** We partition the clean CIFAR-10 dataset among 20 clients using a Dirichlet prior with $\alpha = 0.1$, producing highly imbalanced class proportions. Such label shift typifies FL scenarios where each client serves a niche population—e.g. hospitals specializing in different diseases—violating the IID assumption of standard aggregation rules.

C.3 Detailed Dataset and Model Information

Table. 7 provides a visual overview of the datasets used in this study, categorized by their levels of transformation and data heterogeneity. The table is divided into four sections, corresponding to feature-level, input-level, output-level, and label shift settings:

Feature-Level Shift (Digit5 and DomainNet): The `Digit5` dataset, which consists of digit images collected from five distinct domains, including MNIST, SVHN, USPS, SynthDigits, and MNIST-M. These images exhibit a variety of styles, such as handwritten digits, digits rendered in different fonts, and textured representations, demonstrating substantial visual heterogeneity. The `DomainNet` dataset is a large-scale collection featuring objects and scenes from six domains, including styles like clip art, sketches, and realistic photographs.

Input-Level Shift (`CIFAR10-C` and `CIFAR100-C`): This type of distribution shift includes corrupted versions of CIFAR-10 and CIFAR-100 datasets. The **CIFAR10-C** dataset applies 50 types of corruptions, such as noise, blur, and distortions, to evaluate model robustness under various degradation conditions. Similarly, **CIFAR100-C** extends the CIFAR-100 dataset by introducing the same set of corruptions, enabling robustness evaluation on a larger and more diverse set of categories.

Output-Level Shift (CheXpert and CelebA): The **CheXpert** dataset, a widely used medical imaging dataset labeled for 14 common chest conditions. In this study, the Edema and No Finding labels are grouped, and spurious correlations are introduced at the client level, where attributes (i.e. gender in our client splitting) are disproportionately represented (i.e., 90% of label 1 examples in a client are a certain attribute). The **CelebA** dataset, which includes over 200,000 celebrity faces annotated with 40 attributes. Client splitting follows the same strategy as CheXpert, with attributes such as male, female, blonde hair, and non-blonde hair used to create spurious correlations across clients.

Label Shift (CIFAR10): The final one focuses on label shift in the **CIFAR10** dataset. This setting simulates non-IID conditions by inducing label distributions across clients using a Dirichlet distribution with $\alpha = 0.1$. This creates significant variations in class distributions among the 20 clients, mimicking real-world federated learning scenarios where data availability across clients is inherently imbalanced.

D Further Empirical Results

D.1 Other PEFT Methods Distort Federated Feature

Setup. In this study, we adapted two widely recognized Parameter-Efficient Fine-Tuning (PEFT) methods: LoRA (Hu et al., 2022) and Adapter (Houlsby et al., 2019). Both methods were fine-tuned with meticulous adjustments to their learning rates on the ViT, as detailed in Tab. 8. These configurations allowed us to assess the impact of different fine-tuning strategies on federated features. The performance of each method was measured in terms of local, global, and average accuracy.

(a) Feature-level Shift (`Digit5`and `DomainNet`)

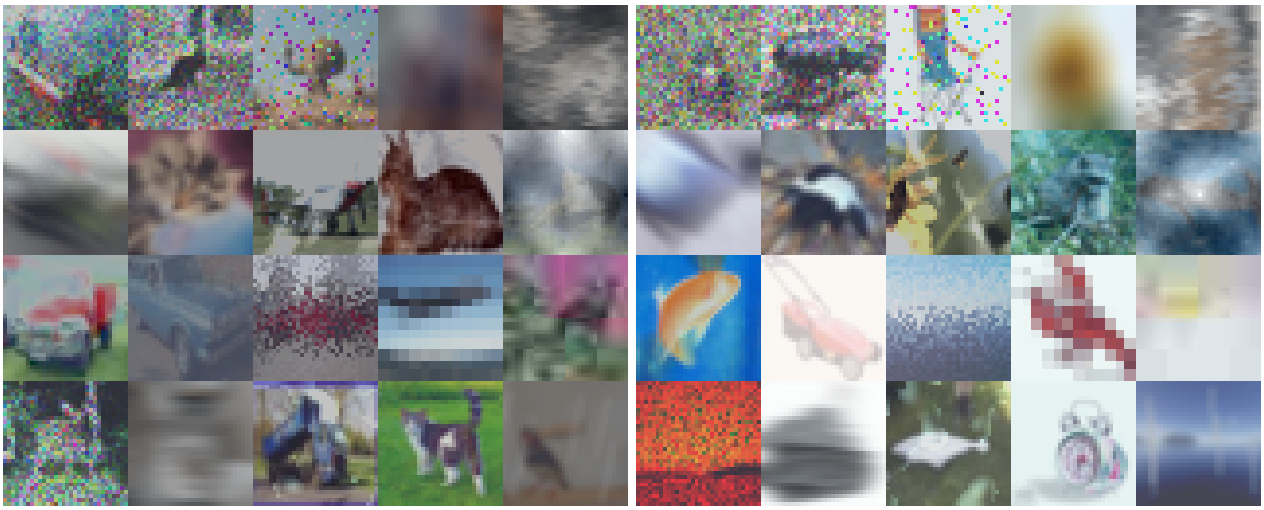

(b) Input-level Shift (`CIFAR10-C` and `CIFAR100-C`)

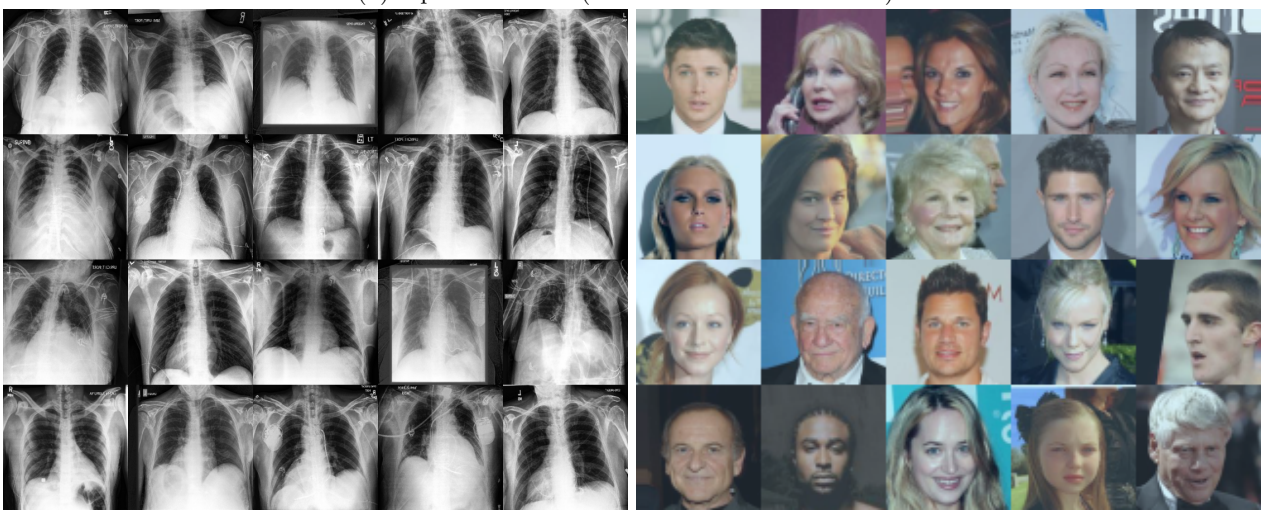

(c) Output-level Shift (`ChexPert` and `CelebA`)

Figure 5: Visualization of the original datasets used in the paper.

Data Heterogeneity Type	Dataset	Model	Description	Clients	Classes
Feature-Level Shift	`Digit5`	ResNet18	A collection of digit images from five domains, used for domain adaptation and digit recognition tasks (Huang et al., 2023). Datasets include MNIST, SVHN, USPS, SynthDigits, and MNIST-M.	5	10
	`DomainNet`	ResNet50	A large-scale dataset of images from six distinct domains for multi-source domain adaptation (Peng et al., 2019b). Preprocessing follows the strategy in FedBN (Li et al., 2021b).	6	10
Input-Level Shift	`CIFAR10-C`	ResNet18	A corruption benchmark dataset for CIFAR-10 (Hendrycks & Dietterich, 2019), augmented with 30 additional corruption types (Mintun et al., 2021) and one extra type (Chen et al., 2021), totaling 50 corruption types (including the original 19 types of corruption from CIFAR-10-C, plus 30 additional corruption types and one extra type, resulting in a total of 50 distinct corruption types).	50	10
	`CIFAR100-C`	ResNet18	An extension of CIFAR-100 with common corruptions, following the same strategy as CIFAR-10-C.	50	100
Output-Level Shift	`CheXpert`	ResNet50	A chest radiograph dataset labeled for 14 common chest conditions (Irvin et al., 2019). Edema and No Finding labels are grouped as described in (Jin et al., 2024). Clients are spuriously correlated with the attribute gender (e.g., 90% of label 1 examples in a client are male).	2	2
	`CelebA`	ResNet50	Over 200,000 celebrity images with 40 attributes (Liu et al., 2015). Client splitting follows the same strategy as CheXpert, with attributes: male, female, blonde hair, and non-blonde hair.	4	2
Label Shift	`CIFAR10`	ResNet18	A benchmark dataset with label shift induced via Dirichlet distribution ($\alpha = 0.1$), distributed across 20 clients (Krizhevsky et al., 2009).	20	10

Table 7: Detailed information about the datasets used in the study. For all the settings above, each client has an individual data distribution, while different clients prohibits the corresponding shifts to ensure the non-IID nature required for heterogeneous FL. Feature-level shift, also referred to as subgroup shift, and input-level shift, corresponding to image corruption, are categorized as covariate shift. Output-level shift, representing spurious correlations in our setting, is categorized as concept shift.

PEFT Method	Local	Global	Avg.
LoRA (lr=1e-3)	41.54	26.75	26.87
LoRA (lr=1e-4)	42.01	26.41	27.18
Adapter (lr=1e-3)	48.35	39.28	38.08
Adapter (lr=1e-4)	49.07	39.83	38.36
LP-FT	68.50	57.52	53.52

Table 8: Different PEFT compared on `DomainNet` with ViT.

Result. The effectiveness of bias tuning in personalized fine-tuning naturally raises the question of whether other PEFT methods, commonly used for fine-tuning large models, exhibit similar effectiveness in our setting. In this study, we compare the local and global performance of other popular PEFT methods. Our findings reveal that while these methods can achieve high levels of local performance, their global performance still

drops significantly, indicating that they distort the federated features to a certain extent. These PEFT methods' local and global performance still fall short compared to LP-FT, indicating that they distort the federated features to a certain extent.

The comparison of PEFT methods in the context of personalized fine-tuning sheds light on the unique challenges and requirements of this setting. Despite the success of PEFT techniques in fine-tuning large models for various tasks, our results suggest that their direct application to personalized FL may not yield optimal results in terms of preserving the global knowledge captured by the federated features.

E Proofs

Proof of Lemma 4.3. We want to analyze the Fine-Tuning (FT) method, focusing on the effect of initial parameters. We perform one pass through the entire dataset to simulate the complete fine-tuning process. Consider the Mean Squared Error (MSE) loss function with parameters V and B, where B is represented as follows:

$$B = \begin{bmatrix} b_1^T \\ \vdots \\ b_m^T \\ b_{m+1}^T \\ \vdots \\ b_{m+C}^T \end{bmatrix},$$

where $b_i^T \in \mathbb{R}^{1\times d}$ denotes the i-th row of matrix B, and $m + C = k$.

To apply one step of gradient descent, we need to compute the gradient of the loss function with respect to V, b_1, b_2, $\ldots$, b_{m+C}, and then perform one update step.

W.L.O.G. we assume the local client is client 1. We define the local loss function as follows:

$$\mathcal{L}_L(V, B) = \mathbb{E}_{x\sim\mathcal{D}_1}\left[\frac{1}{2}(V^T Bx - {V_1^*}^T B_* x)^2\right],$$

where $\mathcal{D}_1$ is the data distribution for client 1.

Now, let $(\mathbf{X}_1, \mathbf{Y}_1)$ represent the local dataset of client 1, consisting of n_1 data points $\{(x_{1j}, y_{1j})\}_{j=1}^{n_1}$. We aim to calculate the gradient of the empirical loss function with respect to the parameters. The empirical loss function is given by:

$$\widehat{\mathcal{L}_L}(V, B) = \frac{1}{n_1}\sum_{j=1}^{n_1}\left[\frac{1}{2}(V^T Bx_{1j} - {V_1^*}^T B_* x_{1j})^2\right].$$

In practice, we take the gradient of this empirical loss function with respect to the parameters V, b_1, b_2, $\ldots$, b_{m+C}. However, since we are particularly interested in computing the expectation $\mathbb{E}[b_j^{FT}]$, we evaluate the expected value of the gradients using one pass through the whole dataset as follows:

$$\begin{aligned}
\mathbb{E}\left[\left.\frac{\partial\widehat{\mathcal{L}_L}}{\partial V}\right|_{\substack{V=V_0\\B=B_*}}\right] &= \mathbb{E}\left[\left.\frac{\partial}{\partial V}\left(\frac{1}{n_1}\sum_{j=1}^{n_1}\frac{1}{2}\left(V^T Bx_{1j} - {V_1^*}^T B_* x_{1j}\right)^2\right)\right|_{\substack{V=V_0\\B=B_*}}\right] \\
&= \frac{1}{n_1}\sum_{j=1}^{n_1}\mathbb{E}\left[(V_0^T B_* x_{1j} - {V_1^*}^T B_* x_{1j})x_{1j}^T B_*^T\right] \\
&= \mathbb{E}_{x\sim\mathcal{D}_1}\left[(V_0^T B_* x - {V_1^*}^T B_* x)x^T B_*^T\right].
\end{aligned}$$

This follows because the dataset is drawn i.i.d. from the population, making the empirical gradient an unbiased estimate of the true gradient. Therefore, let $V_0 = \begin{bmatrix}{V_{com}^*}^T & \mathbf{0}^T\end{bmatrix}^T$. It follows that:

$$\mathbb{E}\left[\left.\frac{\partial L}{\partial V}\right|_{\substack{V=V_0\\B=B_*}}\right] = \mathbb{E}_{x\sim\mathcal{D}_1}\left[(V_0^T B_* x - {V_1^*}^T B_* x)x^T B_*^T\right]$$

$$
\begin{aligned}
&= \mathbb{E}_{x\sim\mathcal{D}_1}\Big[\big((V_0 - V_1^*)^T B_* x\big) x^T B_*^T\Big] \\
&= (V_0 - V_1^*)^T B_* \Big(\mathbb{E}_{x\sim\mathcal{D}_1}\Big[xx^T\Big]\Big) B_*^T \\
&= (V_0 - V_1^*)^T B_* B_*^T && \text{(second moment is identity)} \\
&= (V_0 - V_1^*)^T. && (B_* \text{ has orthonormal rows})
\end{aligned}
$$

Let $B_* = \begin{bmatrix} {b_1^*}^T \\ \vdots \\ {b_m^*}^T \\ {b_{m+1}^*}^T \\ \vdots \\ {b_{m+C}^*}^T \end{bmatrix}$. Then, similarly, it can be shown that:

$$
\begin{aligned}
\mathbb{E}\left[\left.\frac{\partial L}{\partial b_j}\right|_{\substack{V=V_0\\B=B_*}}\right] &= \mathbb{E}_{x\sim\mathcal{D}_1}\left[(V_0^T B_* x - {V_1^*}^T B_* x)(V_0)_j x^T\right] \\
&= \mathbb{E}_{x\sim\mathcal{D}_1}\left[(V_0)_j \Big((V_0 - V_1^*)^T B_* x\Big) x^T\right] \\
&= (V_0)_j (V_0 - V_1^*)^T B_* \Big(\mathbb{E}_{x\sim\mathcal{D}_1}\left[xx^T\right]\Big) \\
&= (V_0)_j (V_0 - V_1^*)^T B_*. && \text{(second moment is identity)}
\end{aligned}
$$

Here, $(V_0)_j$ is the j-th element of the vector V_0. For learning rate η, one step of gradient descent is:

$$
\begin{aligned}
V_{FT} &= V_0 - \eta\left(\left.\frac{\partial L}{\partial V}\right|_{\substack{V=V_0\\B=B_*}}\right)^T \\
b_j^{FT} &= b_j^* - \eta\left(\left.\frac{\partial L}{\partial b_j}\right|_{\substack{V=V_0\\B_0=B_*}}\right)^T.
\end{aligned}
$$

These two equations can be further refined as:

$$
\begin{aligned}
\mathbb{E}\big[V_{FT}\big] &= \begin{bmatrix} {V_{com}^*}^T & \mathbf{0}^T \end{bmatrix}^T - \eta(V_0 - V_1^*) = \begin{bmatrix} {V_{com}^*}^T & \eta\lambda e_1^T \end{bmatrix}^T \\
\mathbb{E}\big[b_j^{FT}\big] &= \mathbb{E}\left[b_j^* - \eta\left(\left.\frac{\partial L}{\partial b_j}\right|_{\substack{V=V_0\\B_0=B_*}}\right)^T\right] = b_j^* - \eta\Big((V_0)_j (V_0 - V_1^*)^T B_*\Big)^T \\
&= b_j^* - \eta\lambda\Big((V_0)_j \begin{bmatrix} \mathbf{0}^T & -e_1^T \end{bmatrix} B_*\Big)^T = b_j^* + \eta\lambda (V_0)_j b_{m+1}^*.
\end{aligned}
$$

Therefore, we have:

$$
\mathbb{E}\Big[B_{FT}\Big] = \begin{bmatrix} {b_1^*}^T + \eta\lambda (V_0)_1 {b_{m+1}^*}^T \\ \vdots \\ {b_m^*}^T + \eta\lambda (V_0)_m {b_{m+1}^*}^T \\ {b_{m+1}^*}^T + \eta\lambda (V_0)_{m+1} {b_{m+1}^*}^T \\ \vdots \\ {b_{m+C}^*}^T + \eta\lambda (V_0)_{m+C} {b_{m+1}^*}^T \end{bmatrix}
$$

$$= \begin{bmatrix} {b_1^*}^T + \eta\lambda(V_0)_1 {b_{m+1}^*}^T \\ \vdots \\ {b_m^*}^T + \eta\lambda(V_0)_m {b_{m+1}^*}^T \\ {b_{m+1}^*}^T \\ \vdots \\ {b_{m+C}^*}^T \end{bmatrix} = \begin{bmatrix} {b_1^*}^T + \eta\lambda(V_{com}^*)_1 {b_{m+1}^*}^T \\ \vdots \\ {b_m^*}^T + \eta\lambda(V_{com}^*)_m {b_{m+1}^*}^T \\ {b_{m+1}^*}^T \\ \vdots \\ {b_{m+C}^*}^T \end{bmatrix}.$$

Similarly, if the fine-tuning is done over the data of client i, we would have:

$$\mathbb{E}\big[b_j^{FT}\big] = b_j^* + \eta\lambda(V_0)_j b_{m+i}^*,$$

which concludes the proof. □

Proof of Theorem 4.4. We assume that the pre-trained model perfectly captures the feature extractor matrix B_*, and its linear head represents the common part shared across all clients, excluding any client-specific components of the ground-truth function. Thus, $B_0 = B_*$ and $V_0 = \begin{bmatrix} {V_{com}^*}^T & \mathbf{0} \end{bmatrix}^T$. In this setting, we analyze the effects of LP-FT and FT on the model parameters. For both LP-FT and FT, we determine the parameters after fine-tuning, compute the global loss, and then compare these global losses.

W.L.O.G. we assume that we are doing the fine-tuning over the local data of client 1. First, we study FT.

It can be shown that:

$$\begin{aligned}
\mathcal{L}_G(V_{FT}, B_{FT}) &= \frac{1}{C}\sum_{i\in[C]} \mathbb{E}_{x\sim\mathcal{D}_i}\left[\frac{1}{2}(V_{FT}^T B_{FT} x - {V_i^*}^T B_* x)^2\right] \\
&= \frac{1}{2C}\sum_{i\in[C]} \mathbb{E}_{x\sim\mathcal{D}_i}\left[(B_{FT}^T V_{FT} - B_*^T V_i^*)^T x x^T (B_{FT}^T V_{FT} - B_*^T V_i^*)\right] \\
&= \frac{1}{2C}\sum_{i\in[C]} (B_{FT}^T V_{FT} - B_*^T V_i^*)^T \Big[\mathbb{E}_{x\sim\mathcal{D}_i}\big[x x^T\big]\Big] (B_{FT}^T V_{FT} - B_*^T V_i^*) \\
&= \frac{1}{2C}\sum_{i\in[C]} (B_{FT}^T V_{FT} - B_*^T V_i^*)^T (B_{FT}^T V_{FT} - B_*^T V_i^*) \qquad \text{(second moment is } I_d) \\
&= \frac{1}{2C}\sum_{i\in[C]} \big\|(B_{FT}^T V_{FT} - B_*^T V_i^*)\big\|_2^2 . \qquad (1)
\end{aligned}$$

We have:

$$\begin{aligned}
B_*^T V_i^* &= \sum_{j=1}^m (V_{com}^*)_j b_j^* + \lambda b_{m+i}^* \\
\mathbb{E}\Big[B_{FT}^T V_{FT}\Big] &= \sum_{j=1}^m (V_{com}^*)_j b_j^* + \sum_{j=1}^m \eta\lambda {(V_{com}^*)_j}^2 b_{m+1}^* + \eta\lambda b_{m+1}^*.
\end{aligned}$$

Therefore, we can obtain:

$$\mathbb{E}\Big[B_{FT}^T V_{FT} - B_*^T V_i^*\Big] = \lambda\Big(\sum_{j=1}^m \eta {(V_{com}^*)_j}^2 b_{m+1}^* + \eta b_{m+1}^* - b_{m+i}^*\Big).$$

For $i \neq 1$, we have:

$$\begin{aligned}
&\mathbb{E}\big[(B_{FT}^T V_{FT} - B_*^T V_i^*)^T (B_{FT}^T V_{FT} - B_*^T V_i^*)\big] \\
&\quad = \lambda^2\big(\sum_{j=1}^m \eta {(V_{com}^*)_j}^2 b_{m+1}^* + \eta b_{m+1}^* - b_{m+i}^*\big)^T \big(\sum_{j=1}^m \eta {(V_{com}^*)_j}^2 b_{m+1}^* + \eta b_{m+1}^* - b_{m+i}^*\big)
\end{aligned}$$

$$= \lambda^2 \left(\left(\eta + \eta \sum_{j=1}^{m} {(V^*_{com})_j}^2 \right)^2 + 1 \right). \qquad \text{(rows of } B_* \text{ are orthonormal)}$$

For $i = 1$, we have:

$$\begin{aligned}
&\mathbb{E}\Big[(B_{FT}^T V_{FT} - B_*^T V_i^*)^T (B_{FT}^T V_{FT} - B_*^T V_i^*)\Big] \\
&\quad = \lambda^2 \big(\sum_{j=1}^{m} \eta {(V^*_{com})_j}^2 b^*_{m+1} + \eta b^*_{m+1} - b^*_{m+i}\big)^T \big(\sum_{j=1}^{m} \eta {(V^*_{com})_j}^2 b^*_{m+1} + \eta b^*_{m+1} - b^*_{m+i}\big) \\
&\quad = \lambda^2 \left(\eta + \eta \sum_{j=1}^{m} {(V^*_{com})_j}^2 - 1 \right)^2. \qquad \text{(rows of } B_* \text{ are orthonormal)}
\end{aligned}$$

Combining these with (1), we can conclude:

$$\begin{aligned}
\mathcal{L}_G(V_{FT}, B_{FT}) &= \mathbb{E}\left[\frac{1}{2C} \sum_{i \in [C]} \left\| (B_{FT}^T V_{FT} - B_*^T V_i^*) \right\|_2^2 \right] \\
&= \frac{\lambda^2}{2C} \left(\left(\eta + \eta \sum_{j=1}^{m} {(V^*_{com})_j}^2 - 1 \right)^2 + (C-1) \left(\left(\eta + \eta \sum_{j=1}^{m} {(V^*_{com})_j}^2 \right)^2 + 1 \right) \right). \qquad (2)
\end{aligned}$$

We can follow the same procedure for LP-FT as follows:

LP step starts from $B_0 = B_*$ and $V_0 = \begin{bmatrix} {V^*_{com}}^T & \mathbf{0} \end{bmatrix}^T$. From proof of Lemma 4.3, we know that $\mathbb{E}\left[\frac{\partial L}{\partial V} \Big|_{\substack{V=V_0 \\ B=B_*}} \right] = (V_0 - V_1^*)^T$. Therefore, after one iteration of LP, we have:

$$V_{LP} = V_0 - \eta \left(\frac{\partial L}{\partial V} \Big|_{\substack{V=V_0 \\ B=B_*}} \right)^T$$

After I iterations we have:

$$\mathbb{E}\big[V_{LP}\big] = \begin{bmatrix} {V^*_{\text{com}}}^\top & \lambda \alpha e_1^\top \end{bmatrix}^\top \qquad \text{for} \qquad \alpha = (1 - (1-\eta)^I)$$

Let the initial parameters after one step of LP and before the FT step be

$$B_{LP} = B_*, \qquad \mathbb{E}\big[V_{LP}\big] \;=\; \begin{bmatrix} {V^*_{\text{com}}}^\top & \lambda \alpha e_1^\top \end{bmatrix}^\top, \quad \alpha \in [0,1].$$

Assume the first client ($i = 1$) runs a single full-batch gradient–descent step with learning–rate η on its local MSE loss. Let V_{LPFT} and B_{LPFT} be the resulting linear head and feature-extractor matrix and $(b_j^{LPFT})^\top$ its j-th row after the final FT step. Then

$$\begin{aligned}
\mathbb{E}\big[V_{LPFT}\big] &= \begin{bmatrix} {V^*_{com}}^T & \lambda\big(\alpha + \eta(1-\alpha)\big) e_1^T \end{bmatrix}^T \\
\mathbb{E}\big[b_j^{LPFT}\big] &= \mathbb{E}\left[b_j^* - \eta \left(\frac{\partial L}{\partial b_j} \Big|_{\substack{V=V_{LP} \\ B_{LP}=B_*}} \right)^T \right] = b_j^* - \eta \left((V_{LP})_j (V_{LP} - V_1^*)^T B_* \right)^T \\
&= b_j^* - \eta\lambda(1-\alpha) \left((V_{LP})_j \begin{bmatrix} \mathbf{0}^T & -e_1^T \end{bmatrix} B_* \right)^T = b_j^* + \eta\lambda(1-\alpha)(V_{LP})_j b^*_{m+1}.
\end{aligned}$$

This steps can be directly obtained exactly as we derived $\mathbb{E}\big[V_{FT}\big]$ and $\mathbb{E}\big[b_j^{FT}\big]$ for FT case.

Similar to computing $\mathcal{L}_G(V_{FT}, B_{FT})$, we find $\mathcal{L}_G(V_{LPFT}, B_{LPFT})$ as follows:

Writing $S := \sum_{j=1}^{m} (V^*_{\text{com}})_j^2 = \|V^*_{\text{com}}\|_2^2$ and

$$A_\alpha := \eta(1-\alpha)S + \big[\alpha + \eta(1-\alpha)\big]\big[1 + \eta\lambda^2\alpha(1-\alpha)\big],$$

the expected global loss

$$\mathcal{L}_G(V_{LPFT}, B_{LPFT}) := \frac{1}{C}\sum_{i=1}^{C} \mathbb{E}_{x\sim\mathcal{D}_i}\Big[\tfrac{1}{2}\big(V_{LPFT}^\top B_{LPFT} x - V_i^{*\top} B_* x\big)^2\Big]$$

satisfies

$$\mathcal{L}_G(V_{LPFT}, B_{LPFT}) \;=\; \frac{\lambda^2}{2C}\Big[(A_\alpha - 1)^2 + (C-1)A_\alpha^2\Big].$$

this is because the LP-FT loss can be obtained similar to FT loss as in (1),

$$\mathcal{L}_G(V_{LPFT}, B_{LPFT}) \;=\; \mathbb{E}\Big[\frac{1}{2C}\sum_{i=1}^{C}\big\|B_{LPFT}^\top V_{LPFT} - B_*^\top V_i^*\big\|_2^2\Big].$$

First, it can be shown that:

$$\mathbb{E}\Big[B_{LPFT}^\top V_{LPFT}\Big] = \sum_{j=1}^{m}(V^*_{\text{com}})_j b_j^* \;+\; \lambda\, A_\alpha\, b_{m+1}^*.$$

For each client $i \in [C]$, $B_*^\top V_i^* = \sum_{j=1}^{m}(V^*_{\text{com}})_j b_j^* + \lambda\, b_{m+i}^*$. Therefore, defining

$$\Delta_i := \mathbb{E}\Big[B_{LPFT}^\top V_{LPFT} - B_*^\top V_i^*\Big],$$

and noting the orthonormality of the rows of B_*, we obtain

$$\|\Delta_i\|_2^2 = \begin{cases} \lambda^2(A_\alpha - 1)^2, & i = 1, \\ \lambda^2 A_\alpha^2, & i \neq 1. \end{cases}$$

Substituting the above norms in the global loss,

$$\mathcal{L}_G(V_{LPFT}, B_{LPFT}) = \frac{\lambda^2}{2C}\Big[(A_\alpha - 1)^2 + (C-1)A_\alpha^2\Big].$$

which is the stated result.

Since we consider convergence for the first (linear probing) step, at convergence we have $\alpha \to 1$, and thus $A_\alpha \to 1$. Therefore, we obtain

$$\mathcal{L}_G(V_{LPFT}, B_{LPFT}) = \frac{\lambda^2}{2C}\big[(A_\alpha - 1)^2 + (C-1)A_\alpha^2\big] \xrightarrow[\alpha\to 1]{} \frac{\lambda^2}{2C}(C-1).$$

In contrast, from (2), we have:

$$\mathcal{L}_G(V_{FT}, B_{FT}) = \frac{\lambda^2}{2C}\left(\left(\eta + \eta\sum\nolimits_{j=1}^{m}{(V^*_{com})_j}^2 - 1\right)^2 + (C-1)\left(\left(\eta + \eta\sum\nolimits_{j=1}^{m}{(V^*_{com})_j}^2\right)^2 + 1\right)\right).$$

Since $\lambda, C \geq 0$, $\big(\eta + \eta\sum_{j=1}^{m}{(V^*_{com})_j}^2 - 1\big)^2 \geq 0$ and $\big(\eta + \eta\sum_{j=1}^{m}{(V^*_{com})_j}^2\big)^2 \geq 0$, each term in $\mathcal{L}_G(V_{FT}, B_{FT})$ exceeds its counterpart in $\mathcal{L}_G(V_{LPFT}, B_{LPFT})$. Hence,

$$\mathcal{L}_G(V_{LPFT}, B_{LPFT}) \leq \mathcal{L}_G(V_{FT}, B_{FT}),$$

which concludes the proof.

□

Proof of Theorem 4.5. W.L.O.G. we assume that the local fine-tuning is performed on the data of the first client. Initially, one step of linear probing is conducted with the fixed feature extractor B_*. After this step, the linear head V_{LP} will converge to V_1^*. This is because we know that:

$$\arg\min_v \left\|\mathbf{X_1}B_0^\top v - \mathbf{X_1}B_*^\top v_*\right\|_2^2 = \left(B_0{\mathbf{X_1}}^\top\mathbf{X_1}B_0^\top\right)^{-1} B_0{\mathbf{X_1}}^\top\mathbf{X_1}B_*^\top v_*,$$

where $\mathbf{X_1}$ is the $n \times d$ matrix including data of n individuals. Since the fine-tuning is on the data of the client 1 (local data), we have:

$$V_{LP} = \left(B_0{\mathbf{X_1}}^\top\mathbf{X_1}B_0^\top\right)^{-1} B_0{\mathbf{X_1}}^\top\mathbf{X_1}B_*^\top V_1^*.$$

Therefore, we have:

$$\begin{aligned}
V_{LP} &= \left(B_0{\mathbf{X_1}}^\top\mathbf{X_1}B_0^\top\right)^{-1} B_0{\mathbf{X_1}}^\top\mathbf{X_1}B_*^\top V_1^* \\
&= \left(B_*{\mathbf{X_1}}^\top\mathbf{X_1}B_*^\top\right)^{-1} B_*{\mathbf{X_1}}^\top\mathbf{X_1}B_*^\top V_1^* \\
&= V_1^*.
\end{aligned}$$

The argument parallels the opening of the proof of Theorem 4.4, where we simulate I iterations of LP. Since at the beginning of the fine-tuning (FT) step, we have the perfect B_* and V_1^* for the local client 1, and FT is performed on the data of the same client, we can conclude that after one step of FT following LP, the parameters will remain unchanged. Specifically, we have $V_{LPFT} = V_1^* = \begin{bmatrix}{V_{com}^*}^T & \lambda e_1^T\end{bmatrix}^T$ and $B_{LPFT} = B_*$.

For the performance on the global data, we have:

$$\begin{aligned}
\mathcal{L}_G(V_{LPFT}, B_{LPFT}) &= \frac{1}{C}\sum_{i\in[C]} \mathbb{E}_{x\sim\mathcal{D}_i}\left[\frac{1}{2}(V_{LPFT}^T B_{LPFT}x - {V_i^*}^T B_* x)^2\right] \\
&= \frac{1}{C}\sum_{i\in[C]} \mathbb{E}_{x\sim\mathcal{D}_i}\left[\frac{1}{2}({V_1^*}^T B_* x - {V_i^*}^T B_* x)^2\right] \\
&= \frac{1}{2C}\sum_{i\in[C]} \mathbb{E}_{x\sim\mathcal{D}_i}\left[(B_*^T V_1^* - B_*^T V_i^*)^T xx^T (B_*^T V_1^* - B_*^T V_i^*)\right] \\
&= \frac{1}{2C}\sum_{i\in[C]} \left[(B_*^T V_1^* - B_*^T V_i^*)^T \mathbb{E}_{x\sim\mathcal{D}_i}\left[xx^T\right](B_*^T V_1^* - B_*^T V_i^*)\right] \\
&= \frac{1}{2C}\sum_{i\in[C]} \left[(V_1^* - V_i^*)^T B_*\left(\mathbb{E}_{x\sim\mathcal{D}_i}\left[xx^T\right]\right)B_*^T(V_1^* - V_i^*)\right] \\
&= \frac{1}{2C}\sum_{i\in[C]} \left[(V_1^* - V_i^*)^T B_*\left(\mathbb{E}_{z\sim\mathcal{N}(0,I_d)}\left[(e_i+\epsilon z)(e_i+\epsilon z)^T\right]\right)B_*^T(V_1^* - V_i^*)\right] \\
&= \frac{1}{2C}\sum_{i\in[C]} \left[(V_1^* - V_i^*)^T B_*\left(e_i e_i^T + \epsilon^2\mathbb{E}_{z\sim\mathcal{N}(0,I_d)}\left[zz^T\right]\right)B_*^T(V_1^* - V_i^*)\right] \\
&= \frac{1}{2C}\sum_{i\in[C]} \left[(V_1^* - V_i^*)^T B_*\left(e_i e_i^T + \epsilon^2 I_d\right)B_*^T(V_1^* - V_i^*)\right] \\
&= \frac{1}{2C}\sum_{i\in[C]} \left[(V_1^* - V_i^*)^T B_*\left(e_i e_i^T\right)B_*^T(V_1^* - V_i^*)\right] \\
&\quad + \frac{1}{2C}\sum_{i\in[C]} \left[(V_1^* - V_i^*)^T B_*\left(\epsilon^2 I_d\right)B_*^T(V_1^* - V_i^*)\right]
\end{aligned}$$

$$
\begin{aligned}
&= \frac{1}{2C}\sum_{i\in[C]}\left[(V_1^*-V_i^*)^T(B_*)_{:,i}(B_*)_{:,i}{}^T(V_1^*-V_i^*)\right] && ((B_*)_{:,i}\ i\text{-th column of } B_*)\\
&\quad+\frac{1}{2C}\sum_{i\in[C]}\left[\epsilon^2(V_1^*-V_i^*)^T(V_1^*-V_i^*)\right] && (B_* \text{ has orthonormal rows})\\
&= \frac{\lambda^2}{2C}\sum_{i\in[C]}\left[\Big((B_*)_{m+1,i}-(B_*)_{m+i,i}\Big)^2\right]+\frac{1}{2C}\epsilon^2\sum_{i\in[C]}\left[\left\|(V_1^*-V_i^*)\right\|_2^2\right]\\
&= \frac{\lambda^2}{2C}\sum_{i\in[C]}\left[\Big((B_*)_{m+1,i}-(B_*)_{m+i,i}\Big)^2\right]+\frac{\lambda^2\big(C-1\big)}{C}\epsilon^2. && (3)
\end{aligned}
$$

We want to analyze the fine-tuning (FT) method, focusing on the effect of initial parameters. We perform one pass through the entire dataset to simulate the complete fine-tuning process. Consider the Mean Squared Error (MSE) loss function with parameters V and B, where B is represented as follows:

$$
B=\begin{bmatrix} b_1^T\\ \vdots\\ b_m^T\\ b_{m+1}^T\\ \vdots\\ b_{m+C}^T\end{bmatrix},
$$

where $b_i^T\in\mathbb{R}^{1\times d}$ denotes the i-th row of matrix B, and $m+C=k$.

To apply one step of gradient descent, we need to compute the gradient of the loss function with respect to V, b_1, b_2, $\ldots$, b_{m+C}, and then perform one update step.

Let $V_0=\begin{bmatrix}{V_{com}^*}^T & \mathbf{0}^T\end{bmatrix}^T$. It follows that:

$$
\begin{aligned}
\mathbb{E}\left[\frac{\partial L}{\partial V}\bigg|_{\substack{V=V_0\\B=B_*}}\right] &= \mathbb{E}_{x\sim\mathcal{D}_1}\left[(V_0^TB_*x-{V_1^*}^TB_*x)x^TB_*^T\right]\\
&= \mathbb{E}_{x\sim\mathcal{D}_1}\left[\big((V_0-V_1^*)^TB_*x\big)x^TB_*^T\right]\\
&= (V_0-V_1^*)^TB_*\Big(\mathbb{E}_{x\sim\mathcal{D}_1}\left[xx^T\right]\Big)B_*^T\\
&= (V_0-V_1^*)^TB_*\Big(\mathbb{E}_{z\sim\mathcal{N}(0,I_d)}\left[(e_1+\epsilon z)(e_1+\epsilon z)^T\right]\Big)B_*^T\\
&= (V_0-V_1^*)^TB_*\Big(e_1e_1^T+\epsilon^2I_d\Big)B_*^T\\
&= (V_0-V_1^*)^TB_*\Big(e_1e_1^T\Big)B_*^T+(V_0-V_1^*)^TB_*\Big(\epsilon^2I_d\Big)B_*^T\\
&= (V_0-V_1^*)^TB_*\Big(e_1e_1^T\Big)B_*^T+\epsilon^2(V_0-V_1^*)^T && (B_* \text{ has orthonormal rows})\\
&= (V_0-V_1^*)^T\Big((B_*)_{:,1}(B_*)_{:,1}{}^T\Big)+\epsilon^2(V_0-V_1^*)^T && ((B_*)_{:,1} \text{ is first column of } B_*)\\
&= \Big(-\lambda(B_*)_{m+1,1}\Big)(B_*)_{:,1}^T+\epsilon^2(V_0-V_1^*)^T.
\end{aligned}
$$

Let $B_* = \begin{bmatrix} {b_1^*}^T \\ \vdots \\ {b_m^*}^T \\ {b_{m+1}^*}^T \\ \vdots \\ {b_{m+C}^*}^T \end{bmatrix}$. Then, it can be shown that:

$$
\begin{aligned}
\mathbb{E}\left[\frac{\partial L}{\partial b_j}\bigg|_{\substack{V=V_0 \\ B=B_*}} \right] &= \mathbb{E}_{x\sim\mathcal{D}_1}\left[(V_0^T B_* x - {V_1^*}^T B_* x)(V_0)_j x^T \right] \\
&= \mathbb{E}_{x\sim\mathcal{D}_1}\left[(V_0)_j \Big((V_0 - V_1^*)^T B_* x \Big) x^T \right] \\
&= (V_0)_j (V_0 - V_1^*)^T B_* \Big(\mathbb{E}_{x\sim\mathcal{D}_1}\left[x x^T \right] \Big) \\
&= (V_0)_j (V_0 - V_1^*)^T B_* \Big(\mathbb{E}_{z\sim\mathcal{N}(0,I_d)} \left[(e_1 + \epsilon z)(e_1 + \epsilon z)^T \right] \Big) \\
&= (V_0)_j (V_0 - V_1^*)^T B_* \Big(e_1 e_1^T + \epsilon^2 I_d \Big) \\
&= (V_0)_j (V_0 - V_1^*)^T B_* \Big(e_1 e_1^T \Big) + (V_0)_j (V_0 - V_1^*)^T B_* \Big(\epsilon^2 I_d \Big) \\
&= (V_0)_j (V_0 - V_1^*)^T B_* \Big(e_1 e_1^T \Big) + \epsilon^2 (V_0)_j (V_0 - V_1^*)^T B_*.
\end{aligned}
$$

Here, $(V_0)_j$ is the j-th element of the vector V_0. For learning rate η, one step of gradient descent can be:

$$
\begin{aligned}
V_{FT} &= V_0 - \eta \left(\frac{\partial L}{\partial V}\bigg|_{\substack{V=V_0 \\ B=B_*}} \right)^T \\
b_j^{FT} &= b_j^* - \eta \left(\frac{\partial L}{\partial b_j}\bigg|_{\substack{V=V_0 \\ B_0=B_*}} \right)^T.
\end{aligned}
$$

These two equations can be further refined as:

$$
\begin{aligned}
\mathbb{E}\big[V_{FT}\big] &= \begin{bmatrix} {V_{com}^*}^T & \mathbf{0}^T \end{bmatrix}^T - \eta \Big(-\lambda (B_*)_{m+1,1} (B_*)_{:,1} + \epsilon^2 (V_0 - V_1^*) \Big) \\
&= \begin{bmatrix} V_{com}^* \\ 0 \\ 0 \\ \vdots \\ 0 \end{bmatrix} + \begin{bmatrix} \mathbf{0} \\ \eta\lambda\epsilon^2 \\ 0 \\ \vdots \\ 0 \end{bmatrix} + \eta\lambda (B_*)_{m+1,1} (B_*)_{:,1} \\
\mathbb{E}\big[b_j^{FT}\big] &= b_j^* - \eta \Big((V_0)_j (V_0 - V_1^*)^T B_* \Big(e_1 e_1^T \Big) + \epsilon^2 (V_0)_j (V_0 - V_1^*)^T B_* \Big)^T \\
&= b_j^* + \begin{bmatrix} \eta\lambda (V_0)_j (B_*)_{m+1,1} \\ 0 \\ \vdots \\ 0 \end{bmatrix} + \eta\lambda (V_0)_j \epsilon^2 b_{m+1}^*.
\end{aligned}
$$

Therefore, we have:

$$\mathbb{E}\big[B_{FT}\big] = \begin{bmatrix} {b_1^*}^T + \eta\lambda(V_0)_1\epsilon^2{b_{m+1}^*}^T + \eta\lambda(V_0)_1(B_*)_{m+1,1}e_1^T \\ \vdots \\ {b_m^*}^T + \eta\lambda(V_0)_m\epsilon^2{b_{m+1}^*}^T + \eta\lambda(V_0)_m(B_*)_{m+1,1}e_1^T \\ {b_{m+1}^*}^T + \eta\lambda(V_0)_{m+1}\epsilon^2{b_{m+1}^*}^T + \eta\lambda(V_0)_{m+1}(B_*)_{m+1,1}e_1^T \\ \vdots \\ {b_{m+C}^*}^T + \eta\lambda(V_0)_{m+C}\epsilon^2{b_{m+1}^*}^T + \eta\lambda(V_0)_{m+C}(B_*)_{m+1,1}e_1^T \end{bmatrix}$$

$$= \begin{bmatrix} {b_1^*}^T + \eta\lambda(V_0)_1\epsilon^2{b_{m+1}^*}^T + \eta\lambda(V_0)_1(B_*)_{m+1,1}e_1^T \\ \vdots \\ {b_m^*}^T + \eta\lambda(V_0)_m\epsilon^2{b_{m+1}^*}^T + \eta\lambda(V_0)_m(B_*)_{m+1,1}e_1^T \\ {b_{m+1}^*}^T \\ \vdots \\ {b_{m+C}^*}^T \end{bmatrix}.$$

It can be shown that:

$$\begin{aligned}
\mathcal{L}_G(V_{FT}, B_{FT}) =& \frac{1}{C}\sum_{i\in[C]} \mathbb{E}_{x\sim\mathcal{D}_i}\left[\frac{1}{2}(V_{FT}^T B_{FT}x - {V_i^*}^T B_* x)^2\right] \\
=& \frac{1}{2C}\sum_{i\in[C]} \mathbb{E}_{x\sim\mathcal{D}_i}\left[(B_{FT}^T V_{FT} - B_*^T V_i^*)^T xx^T (B_{FT}^T V_{FT} - B_*^T V_i^*)\right] \\
=& \frac{1}{2C}\sum_{i\in[C]} (B_{FT}^T V_{FT} - B_*^T V_i^*)^T \left[\mathbb{E}_{x\sim\mathcal{D}_i} xx^T\right](B_{FT}^T V_{FT} - B_*^T V_i^*) \\
=& \frac{1}{2C}\sum_{i\in[C]} (B_{FT}^T V_{FT} - B_*^T V_i^*)^T \Big(e_i e_i^T + \epsilon^2 I_d\Big)(B_{FT}^T V_{FT} - B_*^T V_i^*) \\
=& \frac{1}{2C}\sum_{i\in[C]} (B_{FT}^T V_{FT} - B_*^T V_i^*)^T \Big(e_i e_i^T\Big)(B_{FT}^T V_{FT} - B_*^T V_i^*) \\
&+ \frac{1}{2C}\sum_{i\in[C]} (B_{FT}^T V_{FT} - B_*^T V_i^*)^T \Big(\epsilon^2 I_d\Big)(B_{FT}^T V_{FT} - B_*^T V_i^*) \\
=& \frac{1}{2C}\sum_{i\in[C]} (B_{FT}^T V_{FT} - B_*^T V_i^*)^T \Big(e_i e_i^T\Big)(B_{FT}^T V_{FT} - B_*^T V_i^*) \\
&+ \epsilon^2\frac{1}{2C}\sum_{i\in[C]} \big\|(B_{FT}^T V_{FT} - B_*^T V_i^*)\big\|_2^2 .
\end{aligned} \tag{4}$$

We have:

$$B_*^T V_i^* = \sum_{j=1}^{m} (V_{com}^*)_j b_j^* + \lambda b_{m+i}^*$$

$$\mathbb{E}\Big[B_{FT}^T V_{FT}\Big] = \eta\lambda\epsilon^2\sigma^2 b_{m+1}^* + \sum_{j=m+1}^{m+C}\Big(\eta\lambda(B_*)_{m+1,1}(B_*)_{j,1}\Big)b_j^*$$
$$+ \sum_{j=1}^{m}\Big((V_{com}^*)_j + \eta\lambda(B_*)_{m+1,1}(B_*)_{j,1}\Big)\Big(b_j^* + \eta\lambda(V_{com}^*)_j\epsilon^2\sigma^2 b_{m+1}^* + \eta\lambda(V_{com}^*)_j(B_*)_{m+1,1}e_1\Big).$$

Therefore, we can obtain:

$$\mathbb{E}\Big[B_{FT}^T V_{FT} - B_*^T V_i^*\Big] = \sum_{j=1}^{m} (V_{com}^*)_j \Big(b_j^* + \eta\lambda (V_{com}^*)_j \epsilon^2 \sigma^2 b_{m+1}^* + \eta\lambda (V_{com}^*)_j (B_*)_{m+1,1} e_1\Big)$$
$$+ \eta\lambda\epsilon^2\sigma^2 b_{m+1}^* - \lambda b_{m+i}^* + \sum_{j=m+1}^{m+C} \Big(\eta\lambda (B_*)_{m+1,1} (B_*)_{j,1}\Big) b_j^*$$
$$+ \sum_{j=1}^{m} \Big(\eta\lambda (B_*)_{m+1,1} (B_*)_{j,1}\Big) \Big(b_j^* + \eta\lambda (V_{com}^*)_j \epsilon^2 \sigma^2 b_{m+1}^* + \eta\lambda (V_{com}^*)_j (B_*)_{m+1,1} e_1\Big). \quad (5)$$

From equation (3), we observe that $\mathcal{L}_G(V_{LPFT}, B_{LPFT})$ is a monotonically increasing function of λ and as λ approaches zero, $\mathcal{L}_G(V_{LPFT}, B_{LPFT})$ also converges to zero. In contrast, combining equations (4) and (5), we find that $\mathcal{L}_G(V_{FT}, B_{FT})$ does not converge to zero as λ approaches zero due to the presence of constant terms independent of λ. Therefore, it follows that there always exists a threshold λ^* such that for all $\lambda \leq \lambda^*$:

$$\mathcal{L}_G(V_{LPFT}, B_{LPFT}) \leq \mathcal{L}_G(V_{FT}, B_{FT}).$$

□

F Empirical Performance of LP-FT and FT Under Theorem 4.5 Conditions

To give a better understanding of Theorem 4.5, we give a simple visualization of two randomly generated data-generating functions for different clients and compute the global loss of LP-FT and FT based on equations (3) and (4).

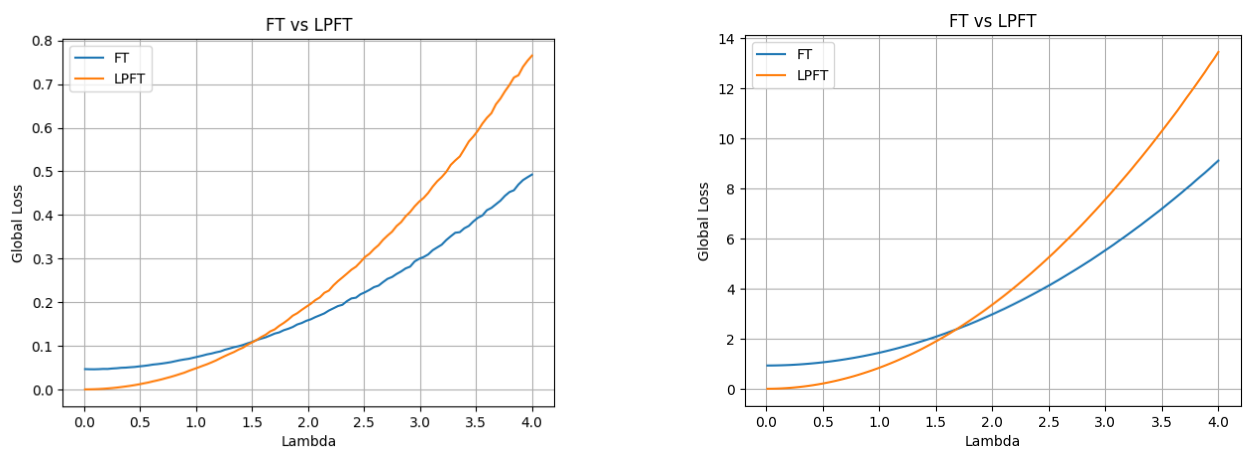

Figure 6: (a) Global loss of LP-FT and FT as a function of the heterogeneity parameter λ, with $\eta = 0.1$, $\epsilon = 0.1$, matrix B_* as a 10×20 random matrix, and number of clients $C = 5$. (b) Global loss of LP-FT and FT as a function of the heterogeneity parameter λ, with $\eta = 0.1$, $\epsilon = 1$, matrix B_* as a 10×20 random matrix, and number of clients $C = 5$.

These examples illustrate, within the theoretical setting of Sec. 4.2, the behavior of the loss functions for LP-FT and FT with a randomly generated labeling function $y = V_i^{*T} B_* x$, a fixed learning rate η, noise parameter ϵ, and a fixed number of clients C. To compute this, we generated 1000 random matrices B_* and 1000 randomly chosen linear heads V_i^* as ground-truth labeling functions, ensuring they adhere to the theoretical assumptions. Using equations (3) and (4), we calculated the average loss of LP-FT and FT across these random trials.

As shown in Fig. 6, there exists a threshold λ^* such that when $\lambda \leq \lambda^*$, LP-FT consistently outperforms FT. While this is a simplified example with a fixed number of clients, learning rate, noise parameter, and dimensionality of the ground-truth parameters B_* and V_i^*, the observed trend remains similar across different parameter settings. The purpose of this figure is to provide an intuitive understanding of Theorem 4.5 in a controlled, simplified context. More comprehensive experiments in Sec. 5.1 demonstrate that LP-FT globally outperforms FT across a broader range of heterogeneity levels in real-world settings.

G Computational Overhead of LP-FT Relative to FT

In this section, we study the computational cost of adding one step of linear probing (LP) before full fine-tuning (FT) to see how this additional LP step affects total computational cost. Suppose the dimension of the output of the feature extractor layer (i.e., the input to the linear head) is d, and the dimension of the output of the linear head is m. Thus, the linear head is a $d \times m$ linear layer. We assume there are n samples. Throughout, we ignore the bias term, as its computational cost is negligible compared to that of the main matrix operations. Our goal is to determine the additional cost incurred by this LP stage compared to FT.

To estimate the computational cost of training a linear neural network layer with d inputs, m outputs, and n samples, we analyze the steps involved:

Forward pass A linear neural network computes outputs as

$$Y = XW,$$

where $X \in \mathbb{R}^{n \times d}$ is the input matrix (with n samples, each of dimension d), $W \in \mathbb{R}^{d \times l}$ is the weight matrix, and $Y \in \mathbb{R}^{n \times l}$ is the output matrix. The cost of this matrix multiplication is $O(ndl)$.

Backward pass To update W, the gradient of the loss $\mathcal{L}$ with respect to W is

$$\nabla_W \mathcal{L} = X^\top \big(\nabla_Y \mathcal{L}\big).$$

Computing $\nabla_W \mathcal{L}$ involves: computing the gradient of the loss with respect to the outputs Y (cost $O(nl)$), and performing the multiplication $X^\top \big(\nabla_Y \mathcal{L}\big)$ (cost $O(ndl)$).

Weight update If using gradient descent, the cost of updating the weights is $O(dl)$.

Total Computational Cost: The total cost for one forward and backward pass through the data is dominated by $O(ndl)$, which accounts for both forward propagation and gradient computation. If the training involves multiple epochs, the total cost scales as $O(e \cdot ndl)$, where e is the number of epochs. During full fine-tuning, an additional backward pass through the feature extractor incurs a substantially larger cost C_{backbone} per epoch. Therefore, adding an LP stage only increases the total cost by $O(e \cdot ndl)$, which is typically negligible compared to the cost of FT.

Broader Impact

This paper presents work whose goal is to advance the field of Machine Learning. There are many potential societal consequences of our work, none of which we feel must be specifically highlighted here.

Limitation

While our theoretical analysis is limited to concept and combined concept-covariate shifts under simplified assumptions (e.g., linear models and shared feature extractors), this does not significantly undermine our contributions. Extensive empirical results across seven diverse datasets demonstrate that LP-FT consistently outperforms baseline methods in both personalization and generalization, even in complex, real-world scenarios. This suggests that the core insights behind LP-FT—such as mitigating feature distortion through phased fine-tuning—generalize well beyond the theoretical scope and offer practical value for robust federated personalization.